Journal of Computational Physics **151,** 74–113 (1999)
Article ID jcph.1999.6202, available online at http://www.idealibrary.com on IDEAL®

Masking Resonance Artifacts in Force-Splitting Methods for Biomolecular Simulations by Extrapolative Langevin Dynamics

Adrian Sandu[1] and Tamar Schlick

Department of Chemistry and Courant Institute of Mathematical Sciences, 251 Mercer Street, New York University and Howard Hughes Medical Institute, New York, New York 10012
E-mail: schlick@nyu.edu

Received July 20, 1998; revised December 22, 1998

Numerical resonance artifacts have become recognized recently as a limiting factor to increasing the timestep in multiple-timestep (MTS) biomolecular dynamics simulations. At certain timesteps correlated to internal motions (e.g., 5 fs, around half the period of the fastest bond stretch, $T_{\min}$), visible inaccuracies or instabilities can occur. Impulse-MTS schemes are vulnerable to these resonance errors since large energy pulses are introduced to the governing dynamics equations when the slow forces are evaluated. We recently showed that such resonance artifacts can be masked significantly by applying extrapolative splitting to stochastic dynamics. Theoretical and numerical analyses of force-splitting integrators based on the Verlet discretization are reported here for linear models to explain these observations and to suggest how to construct effective integrators for biomolecular dynamics that balance stability with accuracy. Analyses for Newtonian dynamics demonstrate the severe resonance patterns of the Impulse splitting, with this severity worsening with the outer timestep, Δt; Constant Extrapolation is generally unstable, but the disturbances do not grow with Δt. Thus, the stochastic extrapolative combination can counteract generic instabilities and largely alleviate resonances with a sufficiently strong Langevin heat-bath coupling (γ), estimates for which are derived here based on the fastest and slowest motion periods. These resonance results generally hold for nonlinear test systems: a water tetramer and solvated protein. Proposed related approaches such as Extrapolation/Correction and Midpoint Extrapolation work better than Constant Extrapolation only for timesteps less than $T_{\min}/2$. An effective extrapolative stochastic approach for biomolecules that balances long-timestep stability with good accuracy for the fast subsystem is then applied to a biomolecule using a three-class partitioning: the medium forces are treated by *Midpoint Extrapolation* via position Verlet, and the slow forces are incorporated by *Constant Extrapolation*.

[1] Present address: Department of Computer Science, Michigan Technological University, Houghton, MI 49931.

0021-9991/99 $30.00

The resulting algorithm (LN) performs well on a solvated protein system in terms of thermodynamic properties and yields an order of magnitude speedup with respect to single-timestep Langevin trajectories. Computed spectral density functions also show how the Newtonian modes can be approximated by using a small γ in the range of 5–20 ps^{-1}.

Key Words: molecular dynamics; numerical resonance; symplecticness; force splitting; multiple timesteps.

1. INTRODUCTION: BIOMOLECULAR SIMULATIONS

With suitable governing force fields and integration protocols, computer simulations of the time evolution of large biomolecular systems can offer insights into molecular flexibility and thermodynamic processes. Yet, the relevance of simulation results to the biological community also depends on the physical timescales that can be simulated. Unfortunately, computer time is a serious handicap in this regard. Namely, the computational cost of biomolecular dynamics simulations is dominated by the frequent (once per timestep) evaluation of the potential energy function and its gradient for a large system. This evaluation frequency cannot be lengthened arbitrarily. Reasonable *accuracy* requires the timestep to be a certain fraction of the period associated with the motion being resolved (e.g., less than one tenth); numerical *stability* dictates an upper bound for the timestep, beyond which trajectories become not only inaccurate but nonsensical; finally, *resonance* artifacts—more erratic disturbances (rather than errors that increase monotonically with the timestep) at selected timesteps related to the natural period of the system—limit the timestep due to their associated inaccuracies and/or instabilities (see below).

For typical single-timestep, unconstrained biomolecular simulations, these three requirements are satisfied by stepsizes in the range of 0.5 to 1 fs. This in turn implies one to two million force evaluations just to span a nanosecond in the life of a biopolymer. As the system size grows, each such evaluation accounts for $\mathcal{O}(N^2)$ interactions, where N is the number of atoms in the system. While approximations are made in practice to reduce the cost of long-range interactions, a nanosecond simulation of a solvated, medium-sized biomolecule (around 20,000 atoms) can require several weeks of computing time on state-of-the-art laboratory workstations. A pioneering 1-μs simulation of a small protein [1] was only possible on a massively parallel Cray supercomputer employed in full for about 4 months.

Despite the large computational work of standard explicit integrators, the Verlet method [2] is often regarded as the "gold standard" of molecular dynamics simulations. Its symplecticness (i.e., volume preserving in phase space; see [3]) and time reversibility are well suited for low-accuracy long-time simulations of Hamiltonian systems; in particular, Verlet trajectories display good energy conservation in comparison to nonsymplectic methods.

1.1. *MTS Approaches and Resonance*

Nearly two decades ago, multiple-timestep (MTS) methods were introduced [4, 5] in an effort to reduce the computational costs of dynamic simulations. MTS methods rely on the observation that the fastest components of the force, which limit the stepsize to 0.5–1 fs, act on a relatively small spatial scale and hence have linear complexity. In contrast, the effort to calculate the slow, long-range interactions increases with the square of the number of

particles. This spatial and temporal division can be exploited by using small timesteps ($\Delta\tau$) to resolve the rapidly varying vibrational modes and larger time intervals (Δt) to update the costly long-range forces.

In the early to mid 1990s, these approaches were further developed and applied to biomolecular dynamics [6–9]. Many of these developments relied on the rigorous and general factorization formalism (disparate timescales, masses, etc.) of the r-RESPA method based on the Trotter factorization [6], a special case of which is the Verlet-I method [7]. These methods are symplectic [3] and time reversible, and thus are intended to simulate accurately Hamiltonian dynamics. The requirement for symplecticness dictates that the slow forces be incorporated via *impulses*, that is, only at the time of their evaluation; hence the name *Impulse-MTS*. These force-splitting schemes also provide modest computational speedup (factors of 4–5) [9] over single-timestep trajectories since savings are realized from updating the long-range forces less frequently than the rapidly varying components.

Yet, the outer timestep (long-range force update interval) in Impulse-MTS cannot be lengthened as might be expected based on criteria of reasonable resolution of the *slow* forces. Instead, it was found that the timescale of the *fast* period limits the outer timestep to somewhat less than $T_{\min}/2$ in standard protocols (i.e., half the period of the fastest motion, which is around 10 fs). Though the first applications attributed these disturbances to general inaccuracies, they were later recognized as resonance artifacts [10, 11]. These artifacts have been analyzed in connection with implicit integration schemes such as implicit midpoint [12] and related integrators [13, 14], and with MTS (or force-splitting) schemes [10, 11]. Impulse-MTS schemes [6, 7] are particularly vulnerable to resonances since relatively large energy pulses are introduced to the governing dynamics equations when the slow forces are evaluated. These large pulses in turn lead to incorrect physical behavior of the system, such as overstretching and/or breaking of bonds [12, 14]. The earlier extrapolative force-splitting alternatives were abandoned because of their noted energy drift (a consequence of nonsymplecticness).

1.2. *A Stochastic MTS Approach*

Barth and Schlick have recently developed an alternative nonsymplectic, stochastic approach termed LN [11, 15] that combines force splitting via extrapolation and stochastic dynamics to overcome this resonance barrier. This combination succeeds, as demonstrated on proteins [15], because extrapolation alleviates the severe resonances of the impulse treatment, and the Langevin heat bath counteracts the instabilities (or energy drift) characteristic of extrapolation.

Of course, these additional terms change the nature of the dynamics. Though strictly speaking, "fictitious dynamics" is generated by this approach, it is expected that the configurational states are sampled with Boltzmann probabilities. Hence the stochastic methods as described here sample configuration space and are useful for determining thermodynamic and structural information; they should not be used to compute dynamic properties such as rate constants.

The simple Langevin formulation used in LN mimics molecular collisions of a biomolecule coupled to a heat bath. The friction is related to the fluctuating random force through the fluctuation–dissipation theorem; together, these terms are used to maintain thermal equilibrium for the system. By choosing the Langevin frictional constant γ as small as possible, just sufficient to ensure numerical stability, we also suggested how to minimize

the effects introduced by the stochastic terms, not present in pure Newtonian formulations [11, 15]. In practice, setting $5 \leq \gamma \leq 50$ ps^{-1} has been suggested in these works.

The long-time stability of the scheme yields speedups of an order of magnitude over reference simulations [15]. These physical and computational properties are advantageous in numerous applications of biomolecular simulations that address the critical sampling problem (see, for example, the Broyde and Hingerty article in this volume [16]); only applications that aim at specific kinetic measurements such as rates of conformational transitions demand accurate Newtonian integrators. Moreover, it has long been recommended that multiple, shorter dynamic trajectories (started from uncorrelated initial states) be used rather than a single long trajectory for improved statistics on sampling and thermodynamics due to the inherent chaos of biomolecular dynamic simulations. Karplus and co-workers recently demonstrated not only that an individual 5-ns trajectory of a protein (crambin) samples a *fraction* of conformational states generated by 10 shorter 120-ps runs; the *average* structural and dynamic properties over the 10 trajectories differ from those obtained from each run and, moreover, this *ensemble average* resembles the X-ray structure most closely [17]. Clearly, efficient sampling approaches are critically needed for macromolecular studies.

1.3. *Resonance Analyses*

In this work, theoretical analyses are developed for various force-splitting strategies for molecular and Langevin dynamics to explain these resonance observations. More important, the analyses offer guidelines for constructing effective biomolecular integrators that balance stability with accuracy given the pragmatic dilemma mentioned above. The linear analyses started in [11] for a one-dimensional (1D) system were based on the symplectic Euler method. Here we base derivations on the Verlet discretization [2] and compare resonance artifacts of Extrapolation versus Impulse force splitting for both Newtonian and Langevin dynamics. Numerical experiments are also performed for nonlinear systems.

Analyses demonstrate the severe resonance patterns of the Impulse splitting, with this severity worsening with the outer timestep, Δt; the general instability of Constant Extrapolation is also demonstrated, but with disturbances that do not grow with Δt. These resonance patterns generally extend to Langevin dynamics, but stochasticity for the extrapolative treatment can succeed in counteracting generic instabilities and largely alleviating resonances with a sufficiently strong heat-bath coupling (γ). Estimates for γ are derived here based on the extreme motion periods associated with the fast and slow timescales.

We also propose related approaches such as Extended Extrapolation/Correction Cycle, Leap Extrapolation, and Midpoint Extrapolation in an attempt to combine the short-timestep accuracy of the Impulse treatment with the large-timestep stability of Constant Extrapolation. Unfortunately, these variants do not appear to have any practical value over the two standard cases on their own right; they can, however, improve the accuracy of Constant Extrapolation over timesteps less than $T_{\min}/2$. This finding is exploited to balance short-time accuracy with long-time stability in LN by relying on *Midpoint Extrapolation* (via position Verlet) for the medium forces and restricting the medium timestep, Δt_m, to less than $T_{\min}/2$, and treating the long-range forces by *Constant Extrapolation* [15]. Performance of these variants also highlights the limitations of the 1D linear analysis and emphasizes the requirement for analyzing multidimensional linear models and experimenting on nonlinear models. Higher dimensionality combined with nonlinearity only aggravates resonance disturbances.

Results also demonstrate that force-splitting approaches are more effective for systems with disparate timescales. A larger system with a greater spread of relevant motion timescales is more amenable to force splitting because, for example, in an extrapolative/Langevin approach the magnitude of the instability or disturbance is proportional to $T_{\min}/T_{\max}$, the ratio of fast period to slow period. The smaller this ratio the milder the instability. Indeed, the resonance sensitivity of Impulse-MTS for both Newtonian and Langevin dynamics and the long-time stability of the Langevin/extrapolative approach is demonstrated for a solvated protein. We also find that stochasticity delays the first occurrence of resonance in Newtonian Impulse-MTS from half the period to the period.

1.4. *Outline*

In Section 2 we detail the 1D linear model problem and the basic procedure used for Newtonian and Langevin analysis based on the velocity Verlet integration. The 3D linear model (treated numerically) is also described. Experiments with the 3D linear model are important for ruling out methods that appear promising for the 1D case. In Section 3 we analyze Newtonian and Langevin dynamics behavior of the linear 1D model for the Impulse and Extrapolation force-splitting variants (both Constant and Midpoint Extrapolation). Section 4 considers a more general framework for hybrid Impulse/Extrapolation techniques, including Extrapolation/Correction (E/C), Extended Extrapolation/Correction Cycle (EE/CC), and Leap Extrapolation, the latter also with velocity corrections ("Leap Extrapolation/Correction"). A three-class MTS variant combining Midpoint Extrapolation with Constant Extrapolation is then analyzed, to mimic the LN method.

Further results in Section 5 on nonlinear systems—a water tetramer and a solvated protein—confirm our analyses regarding the sensitivity of Impulse treatments to resonances, even in the stochastic case, and the long-time stability of extrapolative stochastic variants. They also explain the good performance of Midpoint Extrapolation on a medium timescale and hence its usefulness in the three-class LN approach. The LN solvated protein simulation is analyzed with respect to thermodynamic averages and computational gains (compared to single-timestep Langevin simulations), as well as spectral densities at two coupling parameters. The spectral density functions show the accurate reproduction of Langevin modes by LN at a larger outer timestep and the reasonable approximation to Newtonian modes at the small γ value (5 ps^{-1}).

Conclusions regarding resonance artifacts in force-splitting schemes and the stochastic/extrapolation alternative are presented in Section 6. Much of the detailed numerical analyses are collected in the appendixes. Readers interested in the main findings relevant to biomolecules are directed to the solvated protein subsection (5.2) and the summary (Section 6).

2. LINEAR MODELS FOR MTS ANALYSIS

A linear model is a starting point for MTS analysis since the fast forces are near harmonic and oscillatory. For this reason, numerical experiments performed in conjunction with LIN and its variants [18–20] have shown that, in a large number of systems of real interest, the fast forces can be replaced by linear approximations, with good overall results, provided that the linear approximations are updated often. Still, a 1D linear model has limitations: because of commutativity, it does not capture multidimensional linear behavior. A comparison of results between the 1D and 3D linear models emphasizes this limitation.

2.1. *1D Linear Model*

2.1.1. Newtonian dynamics. Consider the simple 1D linear model problem used by Barth and Schlick [15, 11]:

$$\begin{cases} \dot{X} = V \\ \dot{V} = -(\lambda_1 + \lambda_2)X. \end{cases} \tag{2.1}$$

The variables X and V denote the scalar position and velocity, respectively, for a particle of unit mass. This system can be considered a harmonic oscillator driven by a linear force with constant $\Lambda = \lambda_1 + \lambda_2$. However, we set the scalars $\lambda_2 \ll \lambda_1$ to represent two motion components differing in timescales.

The characteristic angular frequencies associated with the two components and the total motion are respectively

$$\omega_1 = \sqrt{\lambda_1}, \qquad \omega_2 = \sqrt{\lambda_2}, \qquad \Omega = \sqrt{\Lambda}. \tag{2.2}$$

The associated characteristic periods are thus

$$T_1 = \frac{2\pi}{\omega_1}, \qquad T_2 = \frac{2\pi}{\omega_2}, \qquad T = \frac{2\pi}{\Omega}. \tag{2.3}$$

Since $\lambda_2 \ll \lambda_1$, $T_1 \leq T_2 = (\sqrt{\lambda_1/\lambda_2})T_1$; the presence of two (largely different) timescales motivates the use of force-splitting schemes. We set λ_1 and λ_2 so that the fast and slow characteristic periods are $T_1 = 2$ and $T_2 = 10$ (time units) and thus the resonances are easily viewed.

2.1.2. Langevin dynamics. We also consider the Langevin extension of the 1D linear model

$$\begin{cases} \dot{X} = V \\ \dot{V} = -(\lambda_1 + \lambda_2)X - \gamma V + R(t), \end{cases} \tag{2.4}$$

where γ is the friction constant. The random force $R(t)$ has a normal distribution described by

$$\langle R(t) \rangle = 0, \qquad \langle R(t)R(t') \rangle = 2\gamma k_B T \delta(t - t'), \tag{2.5}$$

where T is the temperature, k_B is Boltzmann's constant, and δ is the Dirac function. Since the modeled particle has unit mass, the mass is omitted from the autocovariance expression above.

We also consider the 1D Langevin model problem

$$\begin{cases} \dot{X} = V \\ \dot{V} = -(\lambda_1 + \lambda_2 + \lambda_3)X - \gamma V + R(t), \end{cases} \tag{2.6}$$

which emulates a three-class partitioning of the force, as in the LN method. The three components correspond to fast, medium, and slow forces.

2.2. *Analysis of the 1D Linear Model*

2.2.1. Newtonian dynamics. Barth and Schlick [15, 11] examined MTS schemes based on the first order symplectic Euler method. Here we formulate methods based on the Velocity Verlet discretization [2, 3]; this integrator propagates the velocities (at half steps) and positions (at integral multiples of the timestep $\Delta\tau$) of the system (2.1) as follows:

$$\begin{aligned} V^{n+\frac{1}{2}} &= V^n - \frac{\Delta\tau}{2}\Lambda X^n \\ X^{n+1} &= X^n + \Delta\tau V^{n+\frac{1}{2}} \\ V^{n+1} &= V^{n+\frac{1}{2}} - \frac{\Delta\tau}{2}\Lambda X^{n+1}. \end{aligned} \tag{2.7}$$

The superscript n refers to the numerical approximations of X and V at time $n\Delta\tau$.

The associated step-to-step propagation operator $\Phi\colon \{X^n, V^n\} \to \{X^{n+1}, V^{n+1}\}$ is defined by the equation

$$\begin{aligned} \begin{bmatrix} X^{n+1} \\ V^{n+1} \end{bmatrix} &= \begin{bmatrix} 1 & 0 \\ -\frac{\Delta\tau}{2}\Lambda & 1 \end{bmatrix} \begin{bmatrix} 1 & \Delta\tau \\ 0 & 1 \end{bmatrix} \begin{bmatrix} 1 & 0 \\ -\frac{\Delta\tau}{2}\Lambda & 1 \end{bmatrix} \begin{bmatrix} X^n \\ V^n \end{bmatrix} \\ &= A_{VV}(\Delta\tau, \Lambda) \begin{bmatrix} X^n \\ V^n \end{bmatrix}, \end{aligned} \tag{2.8}$$

where each matrix multiplication corresponds to one sweep through the (2.7) loop. The propagation matrix $A_{VV}(\Delta\tau, \Lambda)$ is symplectic and determines the stability of the method. It can be shown [11] that stability is achieved for

$$\Delta\tau \le 2/\sqrt{\Lambda}. \tag{2.9}$$

This is the familiar linear stability requirement on the timestep of T/π ($T =$ the period) [20]. Throughout this work we assume that the (inner) timestep $\Delta\tau$ obeys this stability restriction.

The following interpretation of Velocity Verlet proves useful later [10]. Let

$$\theta(\Delta\tau, \Lambda) = \arccos\left(1 - \frac{\Delta\tau^2}{2}\Lambda\right), \qquad G(\Delta\tau, \Lambda) = \begin{bmatrix} 1 & 0 \\ 0 & \sqrt{\Lambda\left(1 - \frac{1}{4}(\Delta\tau^2\Lambda)\right)} \end{bmatrix}.$$

Then we factor A_{VV} as

$$A_{VV}(\Delta\tau, \Lambda) = G(\Delta\tau, \Lambda) \begin{bmatrix} \cos\theta & \sin\theta \\ -\sin\theta & \cos\theta \end{bmatrix} G(\Delta\tau, \Lambda)^{-1}$$

to emphasize similarity of A_{VV} to a rotation matrix, a consequence of symplecticness (conservation of area in phase space). The physical angular frequency Ω (Eq. (2.2)) is numerically approximated by an *effective angular frequency* [14, 13]

$$\Omega^{\text{eff}} = \frac{\theta(\Delta\tau, \Lambda)}{\Delta\tau} = \Omega + \mathcal{O}(\Delta\tau^3). \tag{2.10}$$

2.2.2. Langevin dynamics. We analyze the stability and resonance independent of the random force (i.e., $R(t) = 0$), following [15, 11]). We assume that the inner timestep is sufficiently small ($\Delta\tau \to 0$) to justify the asymptotic approximation. Equation (2.4) becomes

$$\ddot{X} + \gamma \dot{X} + \Lambda X = 0$$

(recall $\Lambda = \lambda_1 + \lambda_2$), and admits an analytic solution of the form

$$\begin{bmatrix} X(t) \\ V(t) \end{bmatrix} = e^{-\frac{\gamma t}{2}} A_L(t, \Lambda, \gamma) \begin{bmatrix} X(0) \\ V(0) \end{bmatrix}, \tag{2.11}$$

where $\det(A_L) = 1$. We only consider the underdamped oscillator case ($\gamma^2 < 4\Lambda$), since the overdamped case is not relevant to biomolecules (the position becomes a sum of damped exponentials, with oscillatory characteristics thereby lost). For the underdamped case, the propagator A_L is

$$A_L(t, \Lambda, \gamma) = \begin{bmatrix} \cos(\omega_\gamma t) + \frac{\gamma}{2\omega_\gamma} \sin(\omega_\gamma t) & \frac{1}{\omega_\gamma} \sin(\omega_\gamma t) \\ -\omega_\gamma \left(1 + \frac{\gamma^2}{4\omega_\gamma^2}\right) \sin(\omega_\gamma t) & \cos(\omega_\gamma t) - \frac{\gamma}{2\omega_\gamma} \sin(\omega_\gamma t) \end{bmatrix}, \tag{2.12}$$

where

$$\omega_\gamma = \sqrt{\Lambda - \frac{\gamma^2}{4}}. \tag{2.13}$$

2.3. *3D Linear Model*

Before testing MTS variants on nonlinear problems, we also consider numerical results for a 3D linear model from Biesiadecki and Skeel [10] for three colinear particles (of unit mass) connected by springs of constants k_1 and k_2. The potential energy of this systems is

$$V(r_1, r_2, r_3) = \tfrac{1}{2} k_1 (|r_2 - r_1| - l_1)^2 + \tfrac{1}{2} k_2 (|r_3 - r_2| - l_2)^2,$$

and the corresponding differential equation is

$$\ddot{X} = -\left(\begin{bmatrix} k_1 & -k_1 & 0 \\ -k_1 & k_1 & 0 \\ 0 & 0 & 0 \end{bmatrix} + \begin{bmatrix} 0 & 0 & 0 \\ 0 & k_2 & -k_2 \\ 0 & -k_2 & k_2 \end{bmatrix} \right) X \equiv (K_1 + K_2) X.$$

Since the matrices K_1 and K_2 are not commutative, the system cannot be reduced to three independent 1D models of type (2.1). The system has two fundamental frequencies, $\omega_1 = \sqrt{2k_1}$ and $\omega_2 = \sqrt{2k_2}$, corresponding to the nonzero eigenvalues of K_1 and K_2, respectively. We choose the numerical values $k_1 = \pi^2/2$, $k_2 = \pi^2/50$ to reproduce the fundamental periods $T_1 = 2$ and $T_2 = 10$ used in the 1D linear model above. See also Garcia-Archilla *et al.* [21] for a theoretical stability analysis of a linear multidimensional model.

3. IMPULSE VERSUS EXTRAPOLATION

We now examine the resonance/stability behavior of the Impulse and Extrapolation MTS schemes (the latter in both Constant and Midpoint forms) applied to the linear 1D problem for

both Newtonian and Langevin dynamics. These results are considered graphically alongside those for the 3D linear model.

3.1. *Newtonian Impulse*

Impulse-MTS evaluates the slow force component ($-\lambda_1 X$ here) at timesteps Δt that are k times larger than those ($\Delta\tau$) used for the fast component ($-\lambda_2 X$). We refer to $\Delta\tau$ and $\Delta t = k\Delta\tau$ as the *inner* and the *outer* timesteps, respectively. Impulse Verlet (*"Verlet-I"*) applied to the linear test problem (2.1) becomes

$$
\begin{aligned}
&X^{[0]} = X^n \\
&V^{[0]} = V^n - \tfrac{k\Delta\tau}{2}\lambda_2 X^n \\
&\quad \textbf{For} \quad i = 0 : k-1 \\
&\qquad\quad V^{[i+\frac{1}{2}]} = V^{[i]} - \tfrac{\Delta\tau}{2}\lambda_1 X^{[i]} \\
&\qquad\quad X^{[i+1]} = X^{[i]} + \Delta\tau V^{[i+\frac{1}{2}]} \\
&\qquad\quad V^{[i+1]} = V^{[i+\frac{1}{2}]} - \tfrac{\Delta\tau}{2}\lambda_1 X^{[i+1]} \\
&\quad \textbf{End} \\
&X^{n+1} = X^{[k]} \\
&V^{n+1} = V^{[k]} - \tfrac{k\Delta\tau}{2}\lambda_2 X^{[k]}
\end{aligned}
$$

(Here the superscripts in brackets denote the indices of the inner iterations.) One step of this method advances the solution from $n(k\Delta\tau)$ to $(n+1)(k\Delta\tau)$.

To express the associated propagation matrix A_{IV} for Impulse-Verlet we first introduce the "impulse" matrix

$$
P_{IV}(\Delta\tau, \lambda_2, k) = \begin{bmatrix} 1 & 0 \\ -\frac{k\Delta\tau}{2}\lambda_2 & 1 \end{bmatrix}.
$$

The propagation matrix of Impulse Verlet can then be expressed as

$$
A_{IV}(\Delta\tau, \lambda_1, \lambda_2, k) = P_{IV}(\Delta\tau, \lambda_2, k) A_{VV}(\Delta\tau, \lambda_1)^k P_{IV}(\Delta\tau, \lambda_2, k). \tag{3.1}
$$

The determinant of A_{IV} is one since each of the matrices on the right hand side of (3.1) has unit determinant.

A full theoretical analysis of the resonance is presented in Appendix A. The conclusion is that resonant spikes appear near *multiples of the fast (effective) half period* and their *amplitude increases* with the outer timestep.

3.1.1. Resonance analysis. Numerically computed eigenvalue magnitudes are shown in Fig. 1, as functions of the outer timesteps. Recall that λ_1 and λ_2 in (2.1) were chosen to yield a fast period of 2 time units and a slow period that is five times larger and thereby facilitate the viewing of resonances. We see that the resonant spikes appear to the *left* of integer multiples of the fast half period ($mT_1/2$). The amplitude of the resonant spikes increases linearly with the outer timestep; furthermore, the spikes become wider.

For the 3D linear model, Fig. 2 reveals for Impulse Verlet resonant spikes at odd multiples of the fast half period as expected; however, the other resonant spikes do not appear at even multiples of the fast half period, but approximately at $k\Delta\tau = 1.6$ and 3.2, a behavior not predicted by the 1D model. For sufficiently large outer timesteps the method is unstable.

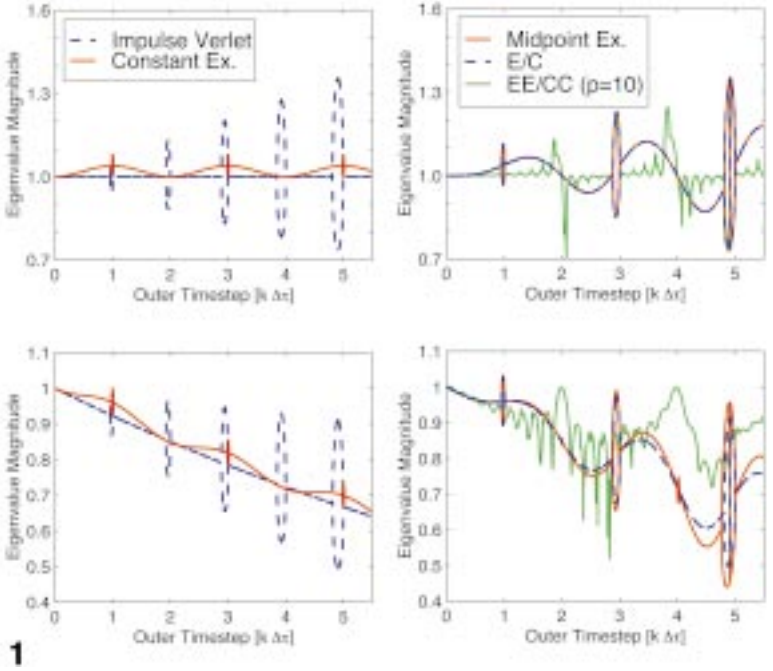

FIG. 1. Eigenvalue magnitudes for the linear 1D test problem with $\Delta\tau = 0.001$, $T_1 = 2$, $T_2 = 10$ for Newtonian (top) and Langevin (bottom) dynamics, $\gamma = 0.162$, of five methods, all shown versus the outer timestep.

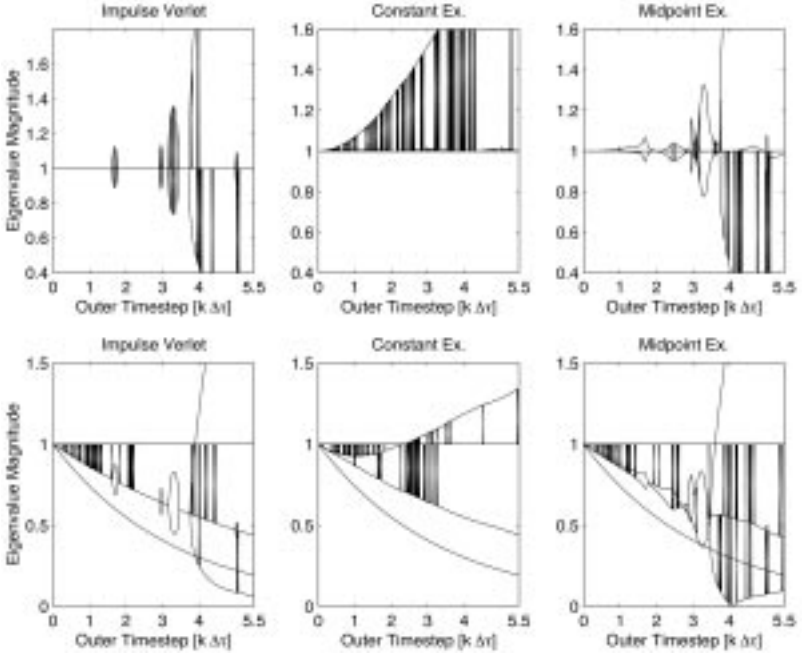

FIG. 2. Eigenvalue magnitudes for the linear 3D test problem for Newtonian (top) and Langevin, $\gamma = 0.3$ (bottom), dynamics, versus the outer timestep, for Impulse, Constant Extrapolation, and Midpoint Extrapolation.

3.1.2. Asymptotic interpretation. Consider now the case when the inner timestep is very small, $\Delta\tau \to 0$, while the outer timestep $k\Delta\tau$ is kept constant. The Impulse Verlet (and in general *any* consistent impulse MTS method) for the 1D linear model becomes

$$
\begin{aligned}
&X^{[0]} = X^n \\
&V^{[0]} = V^n - \tfrac{k\Delta\tau}{2}\lambda_2 X^n \\
&\text{Solve for } 0 \le t \le k\Delta\tau\text{:} \\
&\dot{X} = V,\ \dot{V} = -\lambda_1 X_1, \text{ given} \\
&X(0) = X^{[0]},\ V(0) = V^{[0]}. \\
&X^{n+1} = X(k\Delta\tau) \\
&V^{n+1} = V(k\Delta\tau) - \tfrac{k\Delta\tau}{2}\lambda_2 X(k\Delta\tau).
\end{aligned}
$$

The above system can be solved analytically to obtain the propagator $A^{\mathrm{a}}_{IV} = \partial(X^{n+1}, V^{n+1})/\partial(X^n, V^n)$, which has unit determinant and trace given by

$$\operatorname{trace}\left(A^{\mathrm{a}}_{IV}\right) = 2\cos(\sqrt{\lambda_1}k\Delta\tau) - \frac{k\Delta\tau\lambda_2}{\sqrt{\lambda_1}}\sin(\sqrt{\lambda_1}k\Delta\tau). \tag{3.2}$$

This formula is similar to (A.1) in Appendix A, and the analysis developed there applies. The conclusion is that *no matter which discretization is used for the fast subsystem in an MTS framework the resonant behavior is similar* as long as $\Delta\tau$ is sufficiently small; thus, resonance is inherent to impulse force splitting.

3.2. *Langevin Impulse*

The asymptotic Langevin propagator for Impulse MTS is

$$A^{\mathrm{Lang}}_{IV}(k\Delta\tau, \lambda_1, \lambda_2, \gamma) = e^{-\frac{\gamma k\Delta t}{2}} P_{IV}(\Delta\tau, \lambda_2, k) A_L(k\Delta\tau, \lambda_1, \gamma) P_{IV}(\Delta\tau, \lambda_2, k),$$

and it follows that

$$\det\left(P^{\mathrm{Lang}}_{IV}\right) \equiv \det(P_{IV} A_L P_{IV}) = 1$$

as P^{Lang}_{IV} is the product of matrices of unit determinant. To determine the eigenvalues of P^{Lang}_{IV} and hence the spectrum of A^{Lang}_{IV}, we evaluate the trace of this matrix in the underdamped case ($\gamma < 2\omega_1$),

$$\operatorname{trace}\left(P^{\mathrm{Lang}}_{IV}\right) = 2\cos(\omega_{1,\gamma}k\Delta\tau) - k\Delta\tau\frac{\lambda_2}{\omega_{1,\gamma}}\sin(\omega_{1,\gamma}k\Delta\tau), \tag{3.3}$$

where $\omega_{1,\gamma} = \sqrt{\lambda_1 - \gamma^2/4}$. This trace expression resembles (A.1), and a similar analysis holds. The conclusion is that, for most outer timesteps, the spectrum of A^{Lang}_{IV} consists of a pair of complex conjugate eigenvalues (of modulus $\exp(-\gamma k\Delta\tau/2)$). For outer timesteps close to multiples of the characteristic half period, or

$$k\Delta\tau \approx (m - \beta)\frac{T_{1,\gamma}}{2}, \tag{3.4}$$

where $T_{1,\gamma} = (2\pi)/\omega_{1,\gamma}$, the spectrum of A^{Lang}_{IV} becomes real; that is, the system exhibits resonance artifacts. By substituting (3.4) into (3.3) and estimating the values of β for which the trace is a maximum or a minimum (i.e., those values for which the instability occurs) we obtain

$$\beta \approx \frac{\lambda_2}{\lambda_1}\left(2 + \frac{\lambda_2}{\lambda_1}\right)^{-1} m.$$

This relation indicates the linear increase of spike width with the outer timestep. For this value of β, assuming λ_2/λ_1 is small, we estimate the amplitude of the resonant first spike ($m = 1$) as

$$e^{-\frac{\gamma T_1}{4}}\left(1+\sqrt{2}\pi\frac{\lambda_2}{\lambda_1}\right).$$

For stability, γ must to be large enough to keep the first spike below one. This leads to the following lower bound of γ for numerical stability,

$$\gamma \geq \frac{2\sqrt{\lambda_1}}{\pi}\log\left(1+\frac{\pi}{\sqrt{2}}\frac{\lambda_2}{\lambda_1}\right) = \frac{4}{T_1}\log\left(1+\frac{\pi}{\sqrt{2}}\frac{\lambda_2}{\lambda_1}\right). \tag{3.5}$$

If instead of the asymptotic approximation we consider a numerical implementation, the resonance condition (3.4) involves the "effective half period" $T^{\text{eff}}_{1,\gamma}/2$. In general, the larger the value of γ, the larger $T_{1,\gamma}$ is; thus resonance appears at larger outer timesteps. This is another advantage of using Langevin dynamics.

Numerically calculated eigenvalue magnitudes are shown in Fig. 1 for the 1D linear problem. For large enough values of γ (for which the top of the first spike is less than one) the method is stable. The value $\gamma = 0.162$ used here was calculated from Eq. (3.7) using $\lambda_1 = \pi^2$, $\lambda_2 = \pi^2/25$ (see below). The resonance patterns can be noted with growing severity as Δt increases, as in Newtonian dynamics.

For the 3D linear model (Fig. 2), Impulse force-splitting shows resonance patterns only for larger timesteps, i.e., $\Delta t > 3.5$.

3.3. *Newtonian Constant and Midpoint Extrapolation*

An extrapolative MTS method also evaluates the slow component of the force k times less often than the fast force, but it incorporates an *approximation* of the slow force at each inner timestep. The simplest approximation is based on *Constant Extrapolation*, which calculates the slow forces at the beginning of the outer timestep. The alternative *Midpoint Extrapolation* evaluates the slow component of the force at a coordinate vector that approximates the solution halfway through the Δt sweep; it is reasonable to expect that this variant might yield better resolution of the slow forces for certain protocols. When applied to the linear test problem (2.1), both schemes can be written as

$$\begin{aligned}
&X^{[0]} = X^n\\
&V^{[0]} = V^n\\
&X^{[E]} = \begin{cases} X^{[0]} & [\textit{Constant Extrapolation}]\\ X^{[0]} + (k\Delta\tau/2)V^{[0]} & [\textit{Midpoint Extrapolation}]\end{cases}\\
&\textbf{For}\quad i = 0 : k-1\\
&\qquad V^{[i+\frac{1}{2}]} = V^{[i]} - \tfrac{\Delta\tau}{2}\left(\lambda_1 X^{[i]} + \lambda_2 X^{[E]}\right)\\
&\qquad X^{[i+1]} = X^{[i]} + \Delta\tau V^{[i+\frac{1}{2}]}\\
&\qquad V^{[i+1]} = V^{[i+\frac{1}{2}]} - \tfrac{\Delta\tau}{2}\left(\lambda_1 X^{[i+1]} + \lambda_2 X^{[E]}\right)\\
&\textbf{End}\\
&X^{n+1} = X^{[k]}\\
&V^{n+1} = V^{[k]}.
\end{aligned}$$

We now introduce the matrices

$$E_{CE}(\Delta\tau,\lambda_1,\lambda_2)=\begin{bmatrix} -\frac{1}{2}\Delta\tau^2\lambda_2 & 0 \\ -\Delta\tau\lambda_2+\frac{1}{4}\Delta\tau^3\lambda_1\lambda_2 & 0 \end{bmatrix},$$

$$E_{ME}(\Delta\tau,\lambda_1,\lambda_2)=\begin{bmatrix} -\frac{1}{2}\Delta\tau^2\lambda_2 & -\frac{1}{4}k\Delta\tau^3\lambda_2 \\ -\Delta\tau\lambda_2+\frac{1}{4}\Delta\tau^3\lambda_1\lambda_2 & -\frac{1}{2}k\Delta\tau^2\lambda_2+\frac{1}{8}k\Delta\tau^4\lambda_1\lambda_2 \end{bmatrix},$$

for the Constant and Midpoint Extrapolation variants, respectively, and then express the propagator of Newtonian Extrapolation as

$$A_{**}(\Delta\tau,\lambda_1,\lambda_2,k)=A_{VV}(\Delta\tau,\lambda_1)^k+\sum_{j=0}^{k-1}A_{VV}(\Delta\tau,\lambda_1)^j E_{**}(\Delta\tau,\lambda_1,\lambda_2), \quad (3.6)$$

where $**$ stands for *CE* or *ME* (Constant and Midpoint Extrapolation, respectively).

3.3.1. Resonance analysis. The analyses of the Constant and Midpoint Extrapolation methods are presented in Appendixes B and C, respectively. The main conclusion is that for Constant Extrapolation resonant spikes are *centered* around odd multiples of the effective half period, with *amplitudes independent of the outer timestep* of approximately $1+\lambda_2/\lambda_1$. For Midpoint Extrapolation, resonant spikes occur for outer timesteps *close to, but smaller than,* odd multiples of the effective half period, but the *amplitudes increase with the outer timestep,* as Impulse-MTS. Both methods are unstable for nonresonant timesteps and thus require a stabilizing technique (e.g., a weak coupling to a heat bath) to guarantee numerical stability (and avoid systematic energy drifts) for timesteps that are not small.

The numerically computed eigenvalue magnitudes in Fig. 1 show that Constant Extrapolation is generally unstable. The resonant spikes appear around odd integer multiples of the fast half period ($mT_1/2$) but their amplitude is constant, regardless of the outer timestep. The bottoms of the extrapolation spikes have magnitude unity. For Midpoint Extrapolation, Fig. 1 shows, in contrast, resonant spikes of increasing magnitude. The same generic instability between spikes is seen as for Constant Extrapolation, but for small outer steps (less than one effective quarter period) this instability is very mild.

For the 3D linear problem, both methods are also unstable (Fig. 2), but the instability can be alleviated through stochasticity (see below). The instability of Midpoint Extrapolation at small outer steps is again milder than that for Constant Extrapolation.

3.3.2. Asymptotic interpretation. The analysis for the 1D linear model for Constant Extrapolation is collected in Appendix B, and for Midpoint Extrapolation in Appendix C. We conclude that any consistent integrator with sufficiently small $\Delta\tau$ displays similar resonance patterns: with Constant Extrapolation spike amplitudes are independent of Δt, but with Midpoint Extrapolation they increase with Δt.

3.4. *Langevin Constant and Midpoint Extrapolation*

Any method that discretizes the Langevin equation with Constant and Midpoint Extrapolation approximates (for small $\Delta\tau$) the asymptotic system

$$\ddot{X}+\gamma\dot{X}+\lambda_1 X+\lambda_2 X^{[E]}=0,$$

for $0 \le t \le k\Delta\tau$ and $X(0) = X^0$, $\dot{X}(0) = V^0$, where $X^{[E]}$ was defined for each scheme in the algorithm above. The solution has the form

$$\begin{bmatrix} X(k\Delta\tau) \\ V(k\Delta\tau) \end{bmatrix} = e^{-\frac{\gamma t}{2}} A_{**}^{\text{Lang,a}}(t, \lambda_1, \lambda_2, \gamma) \begin{bmatrix} X^0 \\ V^0 \end{bmatrix},$$

where the subscript $**$ again refers to the method-dependent matrix for Constant (CE) and Midpoint (ME) Extrapolation. Letting $S = \sin(\omega_{1,\gamma} k\Delta\tau)$ and $C = \cos(\omega_{1,\gamma} k\Delta\tau)$, we express the propagator $A_{**}^{\text{Lang,a}}$ for Constant Extrapolation as

$$A_{CE}^{\text{Lang,a}}(k\Delta\tau, \lambda_1, \lambda_2, \gamma) = \begin{bmatrix} \left(1 + \frac{\lambda_2}{\lambda_1}\right)\left(C + \frac{\gamma}{2\omega_{1,\gamma}} S\right) - \frac{\lambda_2}{\lambda_1} e^{\frac{\gamma k\Delta\tau}{2}} & \frac{S}{\omega_{1,\gamma}} \\ -\omega_{1,\gamma}\left(1 + \frac{\lambda_2}{\lambda_1}\right)\left(1 + \frac{\gamma^2}{4\omega_{1,\gamma}^2}\right) S & C - \frac{\gamma}{2\omega_{1,\gamma}} S \end{bmatrix},$$

and for Midpoint Extrapolation as

$$A_{ME}^{\text{Lang,a}} = \begin{bmatrix} \left(1 + \frac{\lambda_2}{\lambda_1}\right)\left(C + \frac{\gamma S}{2\omega_{1,\gamma}}\right) - \frac{\lambda_2}{\lambda_1} e^{\frac{\gamma k\Delta\tau}{2}} & \frac{S}{\omega_{1,\gamma}} + \frac{\lambda_2}{\lambda_1} \frac{k\Delta\tau}{2}\left(\frac{\gamma S}{2\omega_{1,\gamma}} + C - e^{\frac{\gamma k\Delta\tau}{2}}\right) \\ -\omega_{1,\gamma}\left(1 + \frac{\lambda_2}{\lambda_1}\right)\left(1 + \frac{\gamma^2}{4\omega_{1,\gamma}^2}\right) S & C - \frac{\gamma S}{2\omega_{1,\gamma}} + \frac{\lambda_2}{\lambda_1} \frac{k\Delta\tau}{2}\left(1 + \frac{\gamma^2}{4\omega_{1,\gamma}^2}\right) S \end{bmatrix}.$$

For Constant Extrapolation, "resonant" outer timesteps satisfy $k\Delta\tau \approx (2m+1)T_{1,\gamma}/2$; the propagator $\exp(-\gamma k\Delta\tau/2) A_{CE}^{\text{Lang,a}}$ has two real eigenvalues,

$$r_1 = -e^{-\frac{\gamma k\Delta\tau}{2}}, \qquad r_2 = -e^{-\frac{\gamma k\Delta\tau}{2}} - \frac{\lambda_2}{\lambda_1}\left(1 + e^{-\frac{\gamma k\Delta\tau}{2}}\right).$$

Thus, the lower points of each spike lie on the curve $\exp(-\gamma t/2)$, and the amplitude of the spikes is approximately $\lambda_2/\lambda_1(1 + \exp(-\gamma k\Delta\tau/2))$.

Unconditional stability is obtained if all the upper points of the spikes are less than one in absolute value. This reduces to

$$e^{-\frac{\gamma k\Delta\tau}{2}} + \frac{\lambda_2}{\lambda_1}\left(e^{-\frac{\gamma k\Delta\tau}{2}} + 1\right) \le 1 \qquad \Leftrightarrow \qquad \gamma \ge \frac{2\sqrt{\lambda_1}}{\sqrt{\pi^2 + 1}} \log\left(1 + 2\frac{\lambda_2}{\lambda_1}\right).$$

This is a slightly sharper estimate than that given in [15, 11], which was

$$\gamma \ge (2\sqrt{\lambda_1}/\pi) \log(1 + 2\lambda_2/\lambda_1).$$

However, numerical experiments suggest that, while qualitatively correct, neither estimate is sufficient for stability; a practical lower bound (for the linear 1D problem) was empirically found to be

$$\gamma \ge \frac{2\sqrt{\lambda_1}}{\sqrt{\pi^2 - 1}} \log\left(1 + 2\frac{\lambda_2}{\lambda_1}\right) = \frac{4\pi}{T_1\sqrt{\pi^2 - 1}} \log\left(1 + 2\frac{\lambda_2}{\lambda_1}\right), \tag{3.7}$$

a value for which the linear stability was confirmed numerically.

Interestingly, the Langevin formulation introduces a second family of resonances for outer timesteps equal to integer multiples of the characteristic fast period

$$\Delta t \approx m T_{1,\gamma}.$$

For these values the propagator $\exp(-\gamma k\Delta\tau/2)A_{CE}^{\text{Lang,a}}$ has two real eigenvalues,

$$r_1 = e^{-\frac{\gamma k\Delta\tau}{2}}, \qquad r_2 = e^{-\frac{\gamma k\Delta\tau}{2}} + \frac{\lambda_2}{\lambda_1}\left(1 - e^{-\frac{\gamma k\Delta\tau}{2}}\right).$$

At these values the tops of the spikes lie on the curve $\exp(-\gamma t/2)$; the resonant spikes are now below this curve. The amplitudes of the spikes in this case are proportional to $1-\exp(-\gamma k\Delta\tau/2)$, and are clearly much smaller than at odd multiples of the fast period, when they were proportional to $1+\exp(-\gamma k\Delta\tau/2)$.

For Midpoint Extrapolation, resonance occurs when the outer timestep is "near" an odd multiple of the fast half period, i.e., $k\Delta\tau \approx (2m+1-\beta)T_{1,\gamma}/2$, where β is a small positive number; the width of the spike is then $\beta T_{1,\gamma}/2$. The propagator $\exp(-\gamma k\Delta\tau/2)A_{ME}^{\text{Lang,a}}$ has two real eigenvalues,

$$r_1 \approx e^{-\frac{\gamma k\Delta\tau}{2}}\left\{-1 + \left(\frac{\gamma^2}{\omega_{1,\gamma}} + \omega_{1,\gamma}\right)\frac{k\Delta\tau}{2}\beta\pi\right\},$$

$$r_2 \approx -e^{-\frac{\gamma k\Delta\tau}{2}} - \frac{\lambda_2}{\lambda_1}\left(1 + e^{-\frac{\gamma k\Delta\tau}{2}}\right) - e^{-\frac{\gamma k\Delta\tau}{2}}\left(1 + \frac{\lambda_2}{\lambda_1}\right)\left(\frac{\gamma^2}{\omega_{1,\gamma}} + \omega_{1,\gamma}\right)\frac{k\Delta\tau}{2}\beta\pi.$$

This implies that, at large outer timesteps, the method is less stable than Constant Extrapolation.

In Fig. 1 numerical results are shown for Langevin Constant and Midpoint Extrapolation for the 1D model. The value of γ was chosen according to (3.7). Note that the top of the first Constant Extrapolation spike—and hence all spikes—is not greater than one; the Constant Extrapolation method is stable for the 1D linear model. Also note the second family of "small" resonant spikes appearing near multiples of the fast period, a family not present in Newtonian dynamics. For Midpoint Extrapolation the spikes are larger for large outer timesteps.

For small λ_2/λ_1, relation (3.5) predicts the lower bound $\gamma \approx (2\sqrt{2}\pi\lambda_2)/(T_1\lambda_1)$ for the stability of the impulse method, while relation (3.7) gives the bound $\gamma \approx (8\pi\lambda_2)/(\sqrt{\pi^2-1}\,T_1\lambda_1)$ for the stability of Constant Extrapolation. These two bounds have approximately the same magnitude.

The 3D linear model also shows resonance masking through stochasticity (Fig. 2). The value $\gamma \approx 0.162$ estimated by (3.7) stabilizes the Constant Extrapolation scheme for $\Delta t \equiv k\Delta\tau \le T_1/2$; the larger value of $\gamma = 0.3$ renders a stable Constant Extrapolation scheme up to $\Delta t = 2.5$. Larger values of γ will increase the stability range. The bound given by (3.7) was derived to keep the eigenvalue magnitude at $k\Delta\tau = T_1/2$ less than unity. While in the 1D case, this estimate also ensures that the eigenvalue magnitudes for larger outer timesteps are then less than unity, the 3D problem requires a larger γ to maintain stability beyond $T_1/2$. Midpoint Extrapolation shows better stability for small outer timesteps, followed by a sharp rise in eigenvalue magnitude; at large outer steps, it is less stable than Constant Extrapolation.

We suggest in conclusion from this linear analysis that Midpoint Extrapolation might be successfully used in a stochastic framework with small outer timesteps; Constant Extrapolation appears successful with larger outer timesteps provided that the bath coupling parameter γ is strong enough to compensate for inherent instabilities of the method.

4. IMPULSE/EXTRAPOLATION VARIANTS

To combine the benefits of small-timescale accuracy of the Impulse method with the longer-timescale stability of Constant Extrapolation, it is reasonable to consider a combination: the slow force is kept constant during an outer timestep (k inner steps) but, in an attempt to reduce the error introduced by this approximation, velocities are corrected at the beginning and at the end of each outer timestep. The correcting "impulses" have magnitudes equal to the difference between the slow force values at the timestep endpoint and the extrapolative value (the $\mathcal{E}$ term below). These corrections are considerably milder than the pulses used in the pure impulse treatment.

4.1. *General Hybrid Framework*

For the model problem (2.1), one step of Impulse/Constant Extrapolation using an extrapolation value of $\mathcal{E}$ for the slow force reads

$$
\begin{aligned}
&X^{[0]} = X^n \\
&V^{[0]} = V^n + \tfrac{k\Delta\tau}{2}\left(-\lambda_2 X^{[0]} - \mathcal{E}\right) \\
&\quad \textbf{For} \quad i = 0 : k-1 \\
&\qquad V^{[i+\frac{1}{2}]} = V^{[i]} + \tfrac{\Delta\tau}{2}\left(-\lambda_1 X^{[i]} + \mathcal{E}\right) \\
&\qquad X^{[i+1]} = X^{[i]} + \Delta\tau V^{[i+\frac{1}{2}]} \\
&\qquad V^{[i+1]} = V^{[i+\frac{1}{2}]} + \tfrac{\Delta\tau}{2}\left(-\lambda_1 X^{[i+1]} + \mathcal{E}\right) \\
&\quad \textbf{End} \\
&X^{n+1} = X^{[k]} \\
&V^{n+1} = V^{[k]} + \tfrac{k\Delta\tau}{2}\left(-\lambda_2 X^{[k]} - \mathcal{E}\right)
\end{aligned}
$$

If $\mathcal{E}$ is constant throughout the integration, symplectic methods can be obtained (Appendix D). In particular, the choice $\mathcal{E} = 0$ gives the Impulse Verlet method. A natural choice for the extrapolation value $\mathcal{E}$ is the slow force evaluated at some point X^* ($\mathcal{E} = -\lambda_2 X^*$). In this case this variant scheme reads

$$
\begin{aligned}
&X^{[0]} = X^n \\
&V^{[0]} = V^n - \tfrac{k\Delta\tau}{2}\lambda_2\left(X^{[0]} - X^*\right) \\
&\quad \textbf{for} \quad i = 0 : k-1 \\
&\qquad V^{[i+\frac{1}{2}]} = V^{[i]} - \tfrac{\Delta\tau}{2}\left(\lambda_1 X^{[i]} + \lambda_2 X^*\right) \\
&\qquad X^{[i+1]} = X^{[i]} + \Delta\tau V^{[i+\frac{1}{2}]} \\
&\qquad V^{[i+1]} = V^{[i+\frac{1}{2}]} - \tfrac{\Delta\tau}{2}\left(\lambda_1 X^{[i+1]} + \lambda_2 X^*\right) \\
&\quad \textbf{end} \\
&X^{n+1} = X^{[k]} \\
&V^{n+1} = V^{[k]} - \tfrac{k\Delta\tau}{2}\lambda_2\left(X^{[k]} - X^*\right)
\end{aligned}
$$

The theoretical treatment of this hybrid family is facilitated by its resemblance to both Impulse and Constant Extrapolation. We first define the following matrix (which corresponds to the choice $X^* = X^n$ and the *Extrapolation/Correction* [E/C] method),

$$
E_{E/CV}(\Delta\tau, \lambda_2, k) = \begin{bmatrix} 0 & 0 \\ -\frac{k\Delta\tau}{2}\lambda_2 & 0 \end{bmatrix}.
$$

Then the propagator associated with the family is

$$\begin{aligned} E_{IE}(\Delta\tau, \lambda_1, \lambda_2, k) &= -\left(I + P_{IV}(\Delta\tau, \lambda_2, k) A_{VV}^k\right) E_{E/CV}(\Delta\tau, \lambda_2, k) \\ &\quad + P_{IV}(\Delta\tau, \lambda_2, k)\left(\sum_{j=0}^{k-1} A_{VV}^j\right) E_{CE}(\Delta\tau, \lambda_1, \lambda_2) \\ &= I - A_{IV} + P_{IV}(A_{CE} - I)\,. \end{aligned}$$

The updating formula is then

$$\begin{bmatrix} X^{n+1} \\ V^{n+1} \end{bmatrix} = A_{IV}(\Delta\tau, \lambda_1, \lambda_2, k) \begin{bmatrix} X^n \\ V^n \end{bmatrix} + E_{IE}(\Delta\tau, \lambda_1, \lambda_2, k) \begin{bmatrix} X^* \\ V^* \end{bmatrix}. \tag{4.1}$$

The relevant propagator (A_{IE}) depends on the choice of X^*. Holding X^* constant throughout the integration results in a symplectic scheme but then $-\lambda_2 X^*$ can be a poor approximation to $-\lambda_2 X^n$. Adjusting X^* each outer timestep (as in E/C) leads to a better extrapolation, but the nonsymplecticness is reflected in a systematic energy drift.

Another possibility is to update X^* every p outer steps, where p is a chosen integer. We call this method *Extended Extrapolation/Correction Cycle* (EE/CC). This hybrid makes sense for situations where the ratio λ_1/λ_2 is large; reasonable accuracy might then be obtained for a large k ($=\Delta t/\Delta\tau$), but this choice must be balanced with the limit on k due to resonance considerations. The computational complexity of this EE/CC variant does not exceed that for E/C, since the slow forces are still evaluated once each outer timestep.

Finally, the "Leap Extrapolation" variant attempts to achieve a larger range of stability than Constant Extrapolation by symmetrizing the extrapolation process and using a two-step rather than a one-step extrapolation scheme.

We examine these hybrid methods in turn to determine whether they might work better than pure Impulse and Constant Extrapolation.

4.2. *Extrapolation/Correction (E/C)*

The choice $X^* = X^n$ in the above scheme yields impulse velocity corrections after each outer timestep. This approach was considered by several groups to reduce the energy drift of extrapolation [22, 23, 10]; the derivation in [10], in particular, was motivated by the desire to approximate Verlet equivalence [7] for Constant Extrapolation. It has been noted that correcting only for velocities improves numerical performance. This is the version we consider.

When applied to the 1D linear problem (2.1), E/C yields the following protocol:

$$\begin{aligned} &X^{[0]} = X^n \\ &V^{[0]} = V^n \\ &\quad \textbf{For} \quad i = 0 : k-1 \\ &\qquad V^{[i+\frac{1}{2}]} = V^{[i]} - \tfrac{\Delta\tau}{2}\left(\lambda_1 X^{[i]} + \lambda_2 X^{[0]}\right) \\ &\qquad X^{[i+1]} = X^{[i]} + \Delta\tau V^{[i+\frac{1}{2}]} \\ &\qquad V^{[i+1]} = V^{[i+\frac{1}{2}]} - \tfrac{\Delta\tau}{2}\left(\lambda_1 X^{[i+1]} + \lambda_2 X^{[0]}\right) \\ &\quad \textbf{End} \\ &X^{n+1} = X^{[k]} \\ &V^{n+1} = V^{[k]} - \tfrac{k\Delta\tau}{2}\lambda_2\left(X^{[k]} - X^{[0]}\right) \end{aligned}$$

The E/C propagator can be derived directly as

$$A_{E/CV}(\Delta\tau, \lambda_1, \lambda_2, k) = (I + E_{E/CV})A_{CE} - E_{E/CV}, \tag{4.2}$$

or by using $[X^*, V^*] = [X^n, V^n]$ in Eq. (4.1) to obtain (omitting arguments for clarity)

$$A_{IE} = I + P_{IV}(A_{CE} - I) = I + (E_{E/CV} + I)(A_{CE} - I) \equiv A_{E/CV}. \tag{4.3}$$

4.2.1. Resonance analysis. We defer the theoretical analysis to Appendix E. This analysis shows that resonant spikes are centered around odd multiples of the effective half period and that their heights increase almost linearly with the outer timestep. Between resonant spikes, there are additional (nonresonant) instabilities that increase with the outer timestep.

Figure 1 shows the eigenvalue magnitudes for the E/C propagator; the method is generally unstable and performs better than Constant Extrapolation (but not better than Impulse) only for small outer timesteps, say less than $T_1/4$. Resonant spikes appear at *odd* multiples of the fast half period only. Thus, as concluded by Barth and Schlick [11, 15], this hybrid approach seems useful only for small outer timesteps. Results of the Langevin case[2] are shown for reference in Fig. 1; but the method does not appear to have practical utility in its own right though we found it useful in a three-class MTS scheme (see below and in the water tetramer figure).

4.2.2. Asymptotic interpretation. The analysis developed in Appendix E for the 1D model confirms the basic results—good behavior for outer timesteps less than one quarter the fast period and linearly increasing spike amplitudes.

4.3. *Extended Extrapolation/Correction Cycle (EE/CC)*

The EE/CC propagator for p macrosteps is formally written as $A^p_{EE/CC}$ and is defined by

$$\begin{aligned} &A_{EE/CC}(\Delta\tau, \lambda_1, \lambda_2, k)^p \\ &\quad = A_{IV}(\Delta\tau, \lambda_1, \lambda_2, k)^p + \sum_{j=0}^{p-1} A_{IV}(\Delta\tau, \lambda_1, \lambda_2, k)^j E_{IE}(\Delta\tau, \lambda_1, \lambda_2, k) \end{aligned} \tag{4.4}$$

or equivalently

$$\begin{aligned} &A_{EE/CC}(\Delta\tau, \lambda_1, \lambda_2, k)^p \\ &\quad = I + \sum_{j=0}^{p-1} A_{IV}(\Delta\tau, \lambda_1, \lambda_2, k)^j P_{IV}(\Delta\tau, \lambda_2, k)(A_{CE}(\Delta\tau, \lambda_1, \lambda_2, k) - I). \end{aligned} \tag{4.5}$$

A complete theoretical analysis of the resonances of $A_{EE/CC}$ is possible for the 1D linear model but complicated. We restrict our study to the numerically obtained eigenvalues.

In Fig. 1, the absolute values of the spectrum of $A_{EE/CC}$ are plotted as a function of the outer timestep for $p = 1$ (E/C) and $p = 10$ (EE/CC). The curve becomes flatter as p increases, and tends to approximate the Impulse curve. Interesting resonance patterns can

[2] The Langevin propagator of E/C is related to that of the Langevin Constant Extrapolation propagator by the relation $A^{\text{Lang,a}}_{E/CV}(k\Delta\tau, \lambda_1, \lambda_2, \gamma) = (I + E_{E/CV})A^{\text{Lang,a}}_{CE} - E_{E/CV}$. Calculations show that the eigenvalues of $A^{\text{Lang,a}}_{E/CV}$ are resonant for both $k\Delta\tau = (2m+1)T_{1,\gamma}/2$ (large spikes) and $k\Delta\tau = mT_{1,\gamma}$ (small spikes).

also be observed. We conclude that the method is useful only for small outer timesteps and has no advantage over the other splitting variants. We report the Langevin behavior for EE/CC for reference in Fig. 1 for $\gamma = 0.3$, but do not consider the method further; additional experiments substantiate this conclusion.

4.4. *Leap Extrapolation*

Leap Extrapolation is motivated by methods that "symmetrize" the force extrapolation process [24] to obtain stable, long-time integrators for Hamiltonian systems. The name "Leap" is appropriate for the two-step process: we evaluate the slow force at X^n and then advance the numerical solution from $\{X^{n-1}, V^{n-1}\}$ to $\{X^{n+1}, V^{n+1}\}$ while keeping the slow force constant, at its X^n value; in the next step we evaluate the slow force at X^{n+1} and advance the numerical solution from $\{X^n, V^n\}$ to $\{X^{n+2}, V^{n+2}\}$ while keeping the slow force equal to its X^{n+1} value, and so on. When applied to the linear test problem (2.1), Leap Extrapolation reads

$$
\begin{aligned}
&X^{[0]} = X^{n-1}\\
&V^{[0]} = V^{n-1}\\
&\quad\textbf{For}\quad i = 0 : 2k-1\\
&\qquad\quad V^{[i+\frac{1}{2}]} = V^{[i]} - \tfrac{\Delta\tau}{2}\left(\lambda_1 X^{[i]} + \lambda_2 X^n\right)\\
&\qquad\quad X^{[i+1]} = X^{[i]} + \Delta\tau V^{[i+\frac{1}{2}]}\\
&\qquad\quad V^{[i+1]} = V^{[i+\frac{1}{2}]} - \tfrac{\Delta\tau}{2}\left(\lambda_1 X^{[i+1]} + \lambda_2 X^n\right)\\
&\quad\textbf{End}\\
&X^{n+1} = X^{[2k]}\\
&V^{n+1} = V^{[2k]}
\end{aligned}
$$

We also consider a velocity-correcting version ("Leap Extrapolation/Correction"):

$$
\begin{aligned}
&X^{[0]} = X^{n-1}\\
&V^{[0]} = V^{n-1} - k\Delta\tau\lambda_2\left(X^{[0]} - X^n\right)\\
&\quad\textbf{For}\quad i = 0 : 2k-1\\
&\qquad\quad V^{[i+\frac{1}{2}]} = V^{[i]} - \tfrac{\Delta\tau}{2}\left(\lambda_1 X^{[i]} + \lambda_2 X^n\right)\\
&\qquad\quad X^{[i+1]} = X^{[i]} + \Delta\tau V^{[i+\frac{1}{2}]}\\
&\qquad\quad V^{[i+1]} = V^{[i+\frac{1}{2}]} - \tfrac{\Delta\tau}{2}\left(\lambda_1 X^{[i+1]} + \lambda_2 X^n\right)\\
&\quad\textbf{End}\\
&X^{n+1} = X^{[2k]}\\
&V^{n+1} = V^{[2k]} - k\Delta\tau\lambda_2\left(X^{[2k]} - X^n\right)
\end{aligned}
$$

The relevant propagator for the two-step scheme is written as

$$
\begin{bmatrix} X^{n+1}\\ V^{n+1}\\ X^n\\ V^n \end{bmatrix} = \begin{bmatrix} E_{IE}(\Delta\tau, \lambda_1, \lambda_2, 2k) & A_{IV}(\Delta\tau, \lambda_1, \lambda_2, 2k)\\ I & 0 \end{bmatrix} \begin{bmatrix} X^n\\ V^n\\ X^{n-1}\\ V^{n-1} \end{bmatrix}.
$$

It is straightforward to show that the propagator above has a determinant of one if $k\Delta\tau$ is sufficiently small.

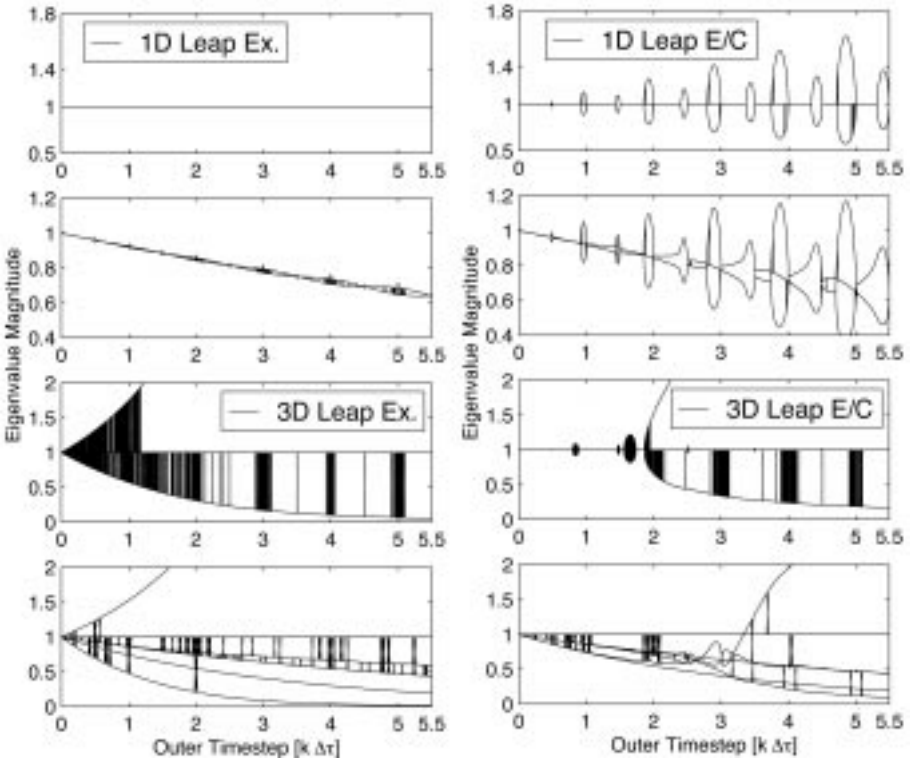

FIG. 3. Eigenvalue magnitudes for the Leap Extrapolation Method (left, Simple; right, Impulse Correction) for the Newtonian 1D Linear Model (first row), Langevin 1D Linear ($\gamma = 0.162$, second row), Newtonian 3D Linear Model (third row), and Langevin 3D Model ($\gamma = 0.3$, last row).

The numerically calculated eigenvalues are presented in Fig. 3 for both the 1D linear and 3D linear models, Newtonian and Langevin dynamics. The non-corrected version (left top) for the 1D model exhibits no resonant spikes; the corrected version (right top) shows large resonant spikes near multiples of the fast half period and, in addition, small resonant spikes at odd multiples of the fast *quarter period*. As characteristic of impulse methods, the heights of the spikes increase with the outer timestep.

Unfortunately, Leap Extrapolation shows a marked instability for the 3D linear model. The Langevin extensions, also shown in Fig. 3 with $\gamma = 0.3$, reveal complex resonance patterns. We thus discard this method, in addition to EE/CC, from further consideration. These hybrids do not appear to offer any practical benefits over Impulse and Constant Extrapolation.

4.5. *Three-Class Splitting by Extrapolation*

Finally, to analyze a three-class extrapolative method as LN [20, 15], we consider the Langevin 1D linear model of system (2.6), where the random force is given by Eq. (2.5). A stochastic extrapolative approach is motivated by the goal of long-time stability and large computational savings rather than accurate Hamiltonian dynamics. In this case, it is advantageous to use a method that yields better accuracy than Constant Extrapolation for the medium force class to improve the accuracy on the medium timescale. Candidates include Extrapolation/Correction (see good behavior in Fig. 1 for $\Delta t < T_1/2$), Impulse, and

Midpoint Extrapolation. We have implemented Midpoint Extrapolation, though limited tests also suggest that the other approaches are effective as long as $\Delta t < T_1/4$. Now we combine Midpoint Extrapolation with Constant Extrapolation in a three-class splitting to obtain for the 1D linear model (2.6) the discretization

$$
\begin{aligned}
&X^{[0,0]} = X^n \\
&V^{[0,0]} = V^n \\
&\textbf{For} \quad j = 0 : k2 - 1 \\
&\quad X^{[E]} = X^{[0,j]} + (k_1 \Delta\tau/2) V^{[0,j]} \\
&\quad \textbf{For} \quad i = 0 : k1 - 1 \\
&\qquad X^{\left[i+\frac{1}{2},j\right]} = X^{[i,j]} + (\Delta\tau/2) V^{[i,j]} \\
&\qquad V^{[i+1,j]} = \left(V^{[i,j]} - \Delta\tau\left(\lambda_1 X^{\left[i+\frac{1}{2},j\right]} + \lambda_2 X^{[E]} + \lambda_3 X^{[0,0]} + R\right)\right) / \left(1 + \gamma\Delta\tau\right) \\
&\qquad X^{[i+1,j]} = X^{\left[i+\frac{1}{2},j\right]} + (\Delta\tau/2) V^{[i+1,j]} \\
&\quad \textbf{End(i)} \\
&\quad X^{[0,j+1]} = X^{[k1,j]} \\
&\quad V^{[0,j+1]} = V^{[k1,j]} \\
&\textbf{End(j)} \\
&X^{n+1} = X^{[k1,k2]} \\
&V^{n+1} = V^{[k1,k2]}
\end{aligned}
$$

Here a triplet of stepsizes $\{\Delta\tau,\ \Delta t_m = k_1\Delta\tau,\ \Delta t = k_2\Delta t_m\}$ is used to integrate the three components of the force. For $\gamma = 0$, the inner iterations reduce to Position Verlet rather than to Velocity Verlet.

For small inner timesteps $\Delta\tau \to 0$, the asymptotic approximation holds, as

$$P_{LN} = A_L + \frac{\lambda_2}{\lambda_1}\left(A_L - e^{\gamma\Delta t_m/2}\right)\begin{bmatrix} 1 & \Delta t_m/2 \\ 0 & 0 \end{bmatrix},$$

where A_L is described in (2.11) and (2.12). Then the propagator matrix associated with the asymptotic approximation is $\exp(-\gamma\Delta t/2)A_{LN}$, where

$$A_{LN} = P_{LN}^{k_2} + \frac{\lambda_3}{\lambda_1}\left(\sum_{i=0}^{k_2-1} e^{(k_2-i-1)\gamma\Delta t_m/2} P_{LN}^i\right)\left(A_L - e^{\gamma\Delta t/2}\right)\begin{bmatrix} 1 & 0 \\ 0 & 0 \end{bmatrix}.$$

Figure 4 shows the eigenvalues of this propagator for different outer timesteps for the chosen periods of $T_1 = 2$, $T_2 = 10$, and $T_3 = 50$ ($\Delta t_m = 0.5$ is used). For the smaller value $\gamma = 0.162$ (left), the eigenvalues of the propagator are quite close to the theoretical values $\exp(-\gamma\Delta t/2)$ (shown in the dashed line). For the larger value $\gamma = 0.3$ (right), one eigenvalue does not decrease with larger outer timesteps. From here we conclude that smaller values of γ might give better averages at large outer timesteps. The fact that the propagator eigenvalues are above their theoretical values means that the LN trajectory will produce a slightly higher energy than the theoretical one. Numerically, we observe a slight rise of the temperature. However, LN is stable for very large outer timesteps.

5. FURTHER EXPERIMENTS

We now experiment with two nonlinear problems: a water tetramer, and the solvated protein bovine pancreatic trypsin inhibitor (BPTI). The purpose of the first model is to

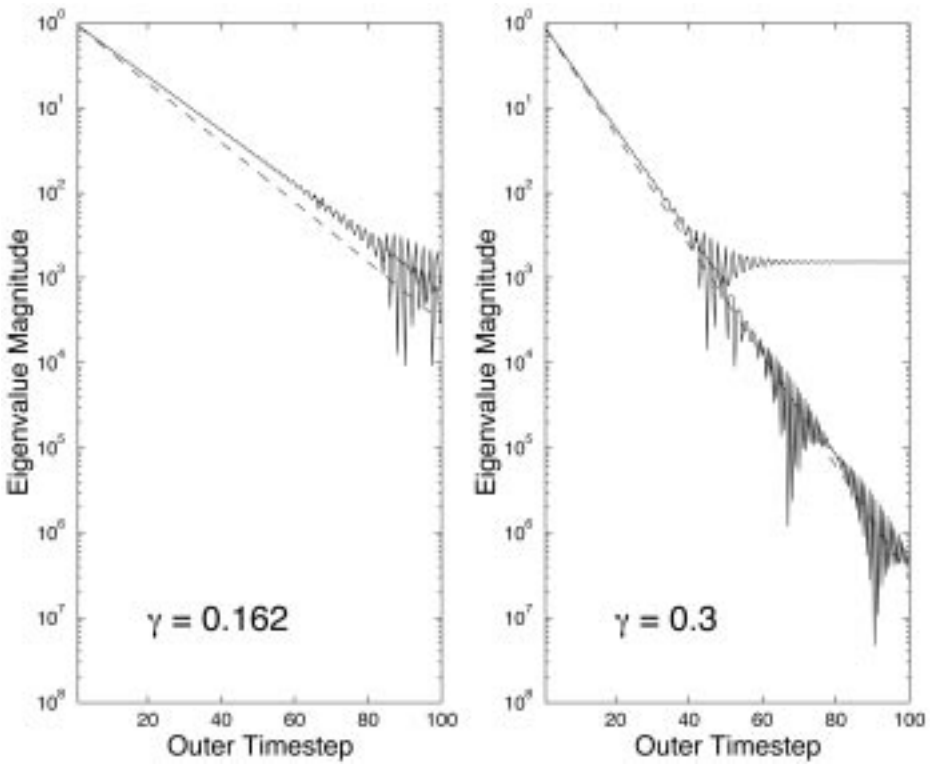

FIG. 4. Eigenvalue magnitudes for the 1D linear model for a three-class Langevin extrapolative splitting with $\gamma = 0.162$ (left) and $\gamma = 0.3$ (right), $\Delta t_m = 0.5$, $T_1 = 2$, $T_2 = 10$, and $T_3 = 50$.

show that the Midpoint Extrapolation hybrid is successful, in the context of a stochastic framework, in removing the first resonant peak of the Impulse method and achieving better accuracy than Constant Extrapolation for outer timesteps less than half the fastest period. The purpose of the second example is to demonstrate an effective three-class stochastic extrapolation strategy for biomolecules that combines Midpoint Extrapolation for the medium forces with Constant Extrapolation for the slow forces.

5.1. *A Water Tetramer*

This test problem is borrowed from Schlick et al. [25], who simulated a flexible water droplet based on standard water potentials. The intermolecular and intramolecular forces correspond to the slowly varying and rapidly varying components, respectively. The intermolecular potential consists of van der Waals and electrostatic terms:

$$E_{\text{inter}}(x) = \sum_{\text{oxygen pairs } (i<j)} \left(\frac{-A}{r_{ij}^6} + \frac{B}{r_{ij}^{12}} \right) + \sum_{\text{atom pairs } (k<l)} \left(\frac{Q_k Q_l}{r_{kl}} \right).$$

The variable r denotes an interatomic distance. The parameters are set as $A = 625.5$ (kcal/mol) Å^6, $B = 629.4 \times 10^3$ (kcal/mol) Å^{12}, $Q_{\text{O}} = -14.94$ (kcal/mol Å)$^{1/2}$, and $Q_{\text{H}} = 7.47$ (kcal/mol Å)$^{1/2}$ (for oxygen and hydrogen atoms).

The intramolecular potential considers bond-length and bond-angle terms for each molecule:

$$E_{\text{intra}}(x) = \sum_{\text{molecules } i} \left(S_1 \sum_{k=1,2} \left(b_{i,k}^2 - \bar{b}^2\right)^2 + S_2(\cos(\theta_i) - \cos(\bar{\theta}_i))^2 \right).$$

Here $\bar{b} = 1$ Å is the equilibrium O–H bond length and $\bar{\theta} = \arccos(-1/3) = 109.471^\circ$ is the equilibrium H–O–H bond angle. The parameters S_1, S_2 have the values $S_1 = 94$ kcal/(mol Å^4), and $S_2 = 42$ kcal/mol.

The initial coordinates and velocities were chosen as described in [25]. A minimum energy configuration was found with the truncated Newton package TNPACK [26–28], followed by an equilibration of the structure at 300 K via a Langevin simulation. From a spectral analysis of the velocity autocorrelation function (as given by a Verlet simulation) we measured that the two fastest frequencies in the system have the associated periods $T_1 \approx 10.8$ fs and $T_2 \approx 21.8$ fs.

The numerical experiments were performed with an inner stepsize of $\Delta\tau = 0.25$ fs and different outer stepsizes for a total time interval of 30 ps. For each run the average and standard deviation of the total energy were recorded. Similar behavior was noted for an inner timestep of 1 fs. The Verlet linear stability condition (2.9) for the intermolecular forces restricts the outer stepsize to ≈6.6 fs. The random force is set at each inner iteration to satisfy the properties given in Eq. (2.5) as (m_i is the mass of atom i)

For $i = 1 : N$
$\quad \text{dev} = \sqrt{(2\gamma k_B m_i T)/(\Delta\tau)}$
$\quad R_i^X = \text{dev} \cdot \text{normal}()$
$\quad R_i^Y = \text{dev} \cdot \text{normal}()$
$\quad R_i^Z = \text{dev} \cdot \text{normal}()$
End

Each call to the function normal() returns a different sample from a normal distribution (with mean 0 and standard deviation 1); for each of the N atoms in the system the three Cartesian components of the random force are obtained by rescaling this distribution to the desired standard deviation.

The results for Langevin Impulse with $\gamma = 20$ ps^{-1} shown in Fig. 5 reveal a resonant spike at an outer timestep value of ≈5.4 fs; for larger timesteps an energy increase due to linear instability is seen. For Constant Extrapolation, the method is linearly unstable, which explains the slow growth of the mean energy as Δt increases. However, no resonant spikes are present and the energy errors increase only slowly with increasing outer timestep. Note that the value of γ suggested by (3.7)—using linearly predicted λ's—is about 150 ps^{-1}. At this value the energy stability would be much better.

The performance of the Langevin Extrapolation/Correction and Midpoint Extrapolation methods shows good energy preservation for small outer timesteps followed by marked instability at larger Δt. At $\Delta t \approx 5.4$ fs, a small resonance occurs. Better behavior than Constant Extrapolation for small outer timesteps can be explained by the second order of consistency (in Δt) of these hybrids. The EE/CC and Leap Extrapolation methods offer no benefits over these variants, as previously concluded: the former gives results similar to those of Impulse splitting, though the first resonant spike at around 5.4 fs is smaller, and the latter yields marked instabilities beyond 4 fs [data not shown].

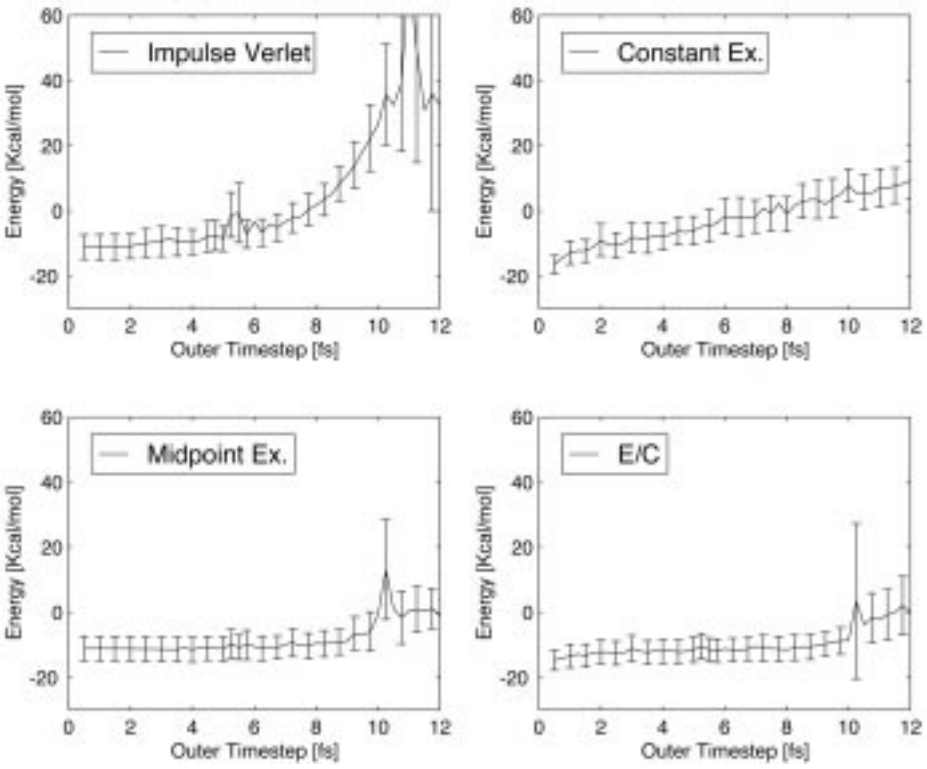

FIG. 5. Water tetramer energy means and deviations over 30-ps Langevin dynamics, $\gamma = 20\ \mathrm{ps}^{-1}$, as a function of the outer timestep for a fixed inner timestep of 0.25 fs.

These experiments thus show that hybrid methods like Midpoint Extrapolation and Extrapolation/Correction can mask the first resonant spike of Impulse in a stochastic framework, but only Constant Extrapolation yields stability at larger outer timesteps.

5.2. *Solvated Bovine Pancreatic Trypsin Inhibitor (BPTI)*

We model the BPTI protein (892 atoms) in CHARMM [29, 30] version 25, solvated in 60 crystallographic and 4401 bulk water molecules (14,275 atoms total). The solvated system was prepared by overlaying the protein atoms on an equilibrated bulk water system (cubic prism of side 70 Å) and then extracting all solvent molecules that included oxygen atoms within 1.8 Å of any heavy protein atom. This system was minimized by steepest descent followed by CHARMM's ABNR minimizer. The final solvated system is a rectangular prism of dimension $60 \times 47 \times 47$ Å^3, modeled with periodic boundary conditions at a cutoff distance of 12 Å. These interactions are truncated using group-based van der Waals potential-shift and electrostatic force-switch functions. The minimized system was heated to 300 K in three successive 10-ps stages using Langevin dynamics with $\gamma = 50$, 10, and 3 ps^{-1}; a similar procedure for setting the random force as described in the previous section is used in CHARMM. The heated system was equilibrated for 20 ps of Newtonian dynamics before production runs began.

The splitting procedure uses three classes and follows Ref. [15]. Namely, bond-length, bond-angle, and dihedral-angle terms are considered fast interactions and resolved at

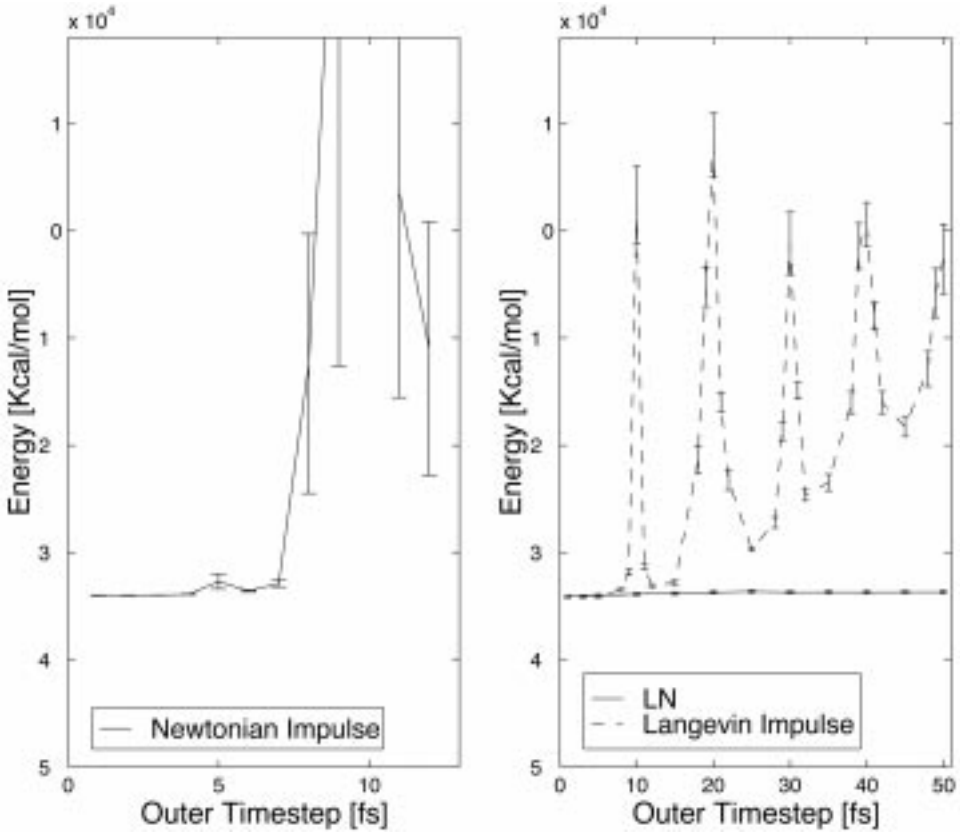

FIG. 6. BPTI energy means and deviations over 5-ps Newtonian dynamics (left), and Langevin dynamics, $\gamma = 20$ ps^{-1} (right), as functions of the outer timestep for a fixed inner timestep of 0.5 fs and medium timestep of 1 fs.

$\Delta\tau = 0.5$ fs; local nonbonded forces (within 7 Å) are considered medium interactions and resolved at $\Delta t_m = 1$ or 2 fs; and all other forces are classified as slow. The medium forces are separated from the slow forces via a smooth force switching function with a 1-Å buffer region; a larger buffer region worsens results. We found that this three-class partitioning worked much better than a two-class scheme. A spectral analysis of this test problem (see below) indicates that the fastest periods in the system are around 10 fs (associated with O–H stretches), 11 fs (C–H stretches), 19 fs (water H–O–H bends), 24 fs, and above (various bending nodes and heavy atom bond vibrations, such as C–C and C=O).

For comparing resonance behavior between impulse and extrapolative variants, the system was integrated for 5 ps with a medium timestep $\Delta t_m = 1$ fs and various outer timesteps for both Newtonian and Langevin ($\gamma = 20$ ps^{-1}) dynamics (Fig. 6). This smaller value of Δt_m was used because Newtonian Impulse does not work well with $\Delta t_m = 2$ fs and Langevin Impulse was also worse at this setting.

Figure 6 shows how resonance appears for Newtonian Impulse at $\Delta t \approx 5$ fs, as predicted by linear theory; for larger outer timesteps, generic instability occurs, as expected. For Langevin/Impulse, we see that the first resonant spike at 5 fs is delayed: the integration is stable for timesteps up to 6 fs, and a strong resonance signal emerges near 10 fs for this γ. Thus, stochasticity succeeds in strongly alleviating the 5-fs resonance for this complex

TABLE I
LN Performance on Solvated BPTI, $\gamma = 20\ \text{ps}^{-1}$, $\Delta\tau = 0.5$ fs, $\Delta t_m = 2$ fs, Δt Varied

Δt	$\langle T\rangle$	$\langle (T-\langle T\rangle)^2\rangle^{1/2}$	$\langle E\rangle$	$\langle (E-\langle E\rangle)^2\rangle^{1/2}$	Speedup
Ref.	298.5	2.0 (0.67%)	−34054.8	121.5 (0.36%)	1
2	300.6	2.1 (0.70%)	−34079.4	145.2 (0.43%)	2.3
10	302.2	2.1 (0.69%)	−33929.0	130.3 (0.38%)	4.3
20	303.7	2.2 (0.72%)	−33687.7	152.7 (0.45%)	6.6
50	302.1	2.1 (0.70%)	−33722.8	160.6 (0.48%)	9.8
100	301.9	1.9 (0.63%)	−33654.7	145.8 (0.43%)	11.7
200	301.7	2.2 (0.73%)	−33450.7	142.2 (0.43%)	13.1

Note. The temperature and energy and their variances are shown, along with the speedup measured relative to the explicit Langevin trajectory in CHARMM at $\Delta\tau$.

system though it did not for the water tetramer for the same γ. The difference in ratios between the extreme timescales (characterized by λ_2/λ_1) for each system is a likely explanation. Namely, for the solvated protein, this ratio is smaller (slower modes are present) and hence the instability amplitude is relatively small. The removal of the 5-fs resonance by the Langevin approach was also shown in [15]. For large outer timesteps, Langevin/Impulse is unstable, with marked resonances at multiples of 10 fs. The LN results, in contrast, are very good for large outer timesteps: energy averages and variances are correct for all values of Δt displayed.

In fact, we found that Δt_m can be increased to 2 fs and Δt to 200 fs without excessively increasing the thermodynamic errors as measured with respect to a single-timestep Langevin trajectory at $\Delta\tau = 0.5$ fs. Results obtained with these settings are reported in Table I (see also [15]) and in the remaining figures.

Figure 7, which presents the errors of the LN trajectory averages relative to the reference trajectory for the various energy components and the temperature, shows that all relative errors remain below 3% for Δt up to 200 fs.

Dynamic properties as a function of γ are next examined. The spectral analyses of the trajectories shown in Fig. 8 for two γ values used data from the first 2 ps of the trajectory at the outer timestep of $\Delta t = 192$ fs sampled every 2 fs. (Very similar results are obtained for all outer timesteps examined, up to 200 fs.) The procedure involves computing the velocity autocorrelation time series for each atom in the system and then Fourier transforming them to obtain a power spectrum for each atom; these spectra are then averaged over the protein atoms and over the water atoms separately for a global characterization of the motion. In more detail, the sampled 2-ps trajectory yields velocity time series $\{v_1^j \ldots v_n^j\}$ for each atom j in the system and each Cartesian coordinate (the subscript is the snapshot time index). We subtract the average quantity to yield

$$v_l^j \leftarrow v_l^j - \frac{1}{n}\sum_{l=1}^{n} v_l^j, \qquad l = 1, \ldots, n,$$

and produce the normalized velocity autocorrelation series covering the 2-ps interval as

$$a_p^j = \frac{\sum_{l=n/2}^{n} v_l^j v_{l-p+1}^j}{\sum_{l=n/2}^{n} v_l^j v_l^j}, \qquad p = 1, \ldots, n/2.$$

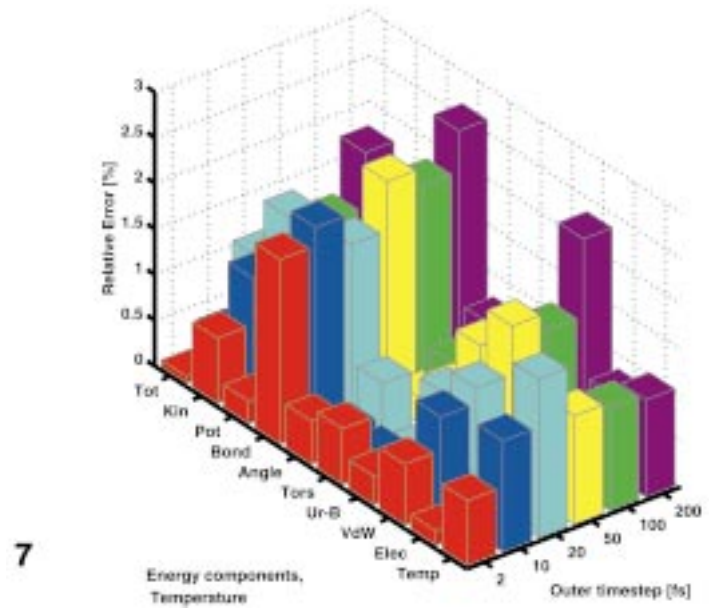

FIG. 7. BPTI relative errors of LN ($\Delta\tau = 0.5$ fs, $\Delta t_m = 2$ fs, Δt varied from 2 to 200 fs) with respect to the reference Langevin trajectory at the single-timestep value $\Delta\tau$ for $\gamma = 20$ ps^{-1}.

This time series is then Fourier transformed to the frequency domain to obtain the (individual) power spectra

$$A_\omega^j = \sum_{p=1}^{n/2} a_p^j e^{i\omega p}, \qquad \omega = 1, \ldots, n/2.$$

These spectra are averaged over the protein and water atoms separately (N_{prot} and N_{wat} below denote the total number of protein and water atoms, respectively):

$$A_\omega^{\text{prot}} = \sum_{j \in \text{prot}} A_\omega^j \,/\, N_{\text{prot}}, \qquad A_\omega^{\text{wat}} = \sum_{j \in \text{wat}} A_\omega^j \,/\, N_{\text{wat}}, \qquad \omega = 1, \ldots, n/2.$$

Not only do we see from Fig. 8 that the LN spectra for the large-timestep trajectory are barely distinguishable from the spectra obtained from the reference, 0.5-fs Langevin trajectory; we observe that the Newtonian modes are smoothed by the stochastic treatment, as expected, and that the smaller value of γ used here leads to a better agreement between Newtonian and Langevin spectra. This effect of γ is illuminated by Fig. 9, which compares the Newtonian to Langevin (LN) spectra at two γ values. Thus, our $\gamma = 5$ and 20 ps^{-1} values, sufficient for numerical stability, do not blur the internal signals grossly.

As for computational speedup, LN produces a factor of 13 for the largest outer timestep (Table I). This is close to the asymptotic upper limit for the present system, since the computational work involved in the slow forces is already less than about 10% and, instead, the evaluation of medium forces has become the dominant computational burden. A further splitting of the medium forces, resulting in a generalization of LN to more than three classes, might be useful to increase the speedup. Additional experiments for a different approach, namely introducing the slow forces via linear extrapolation, show that this does not work

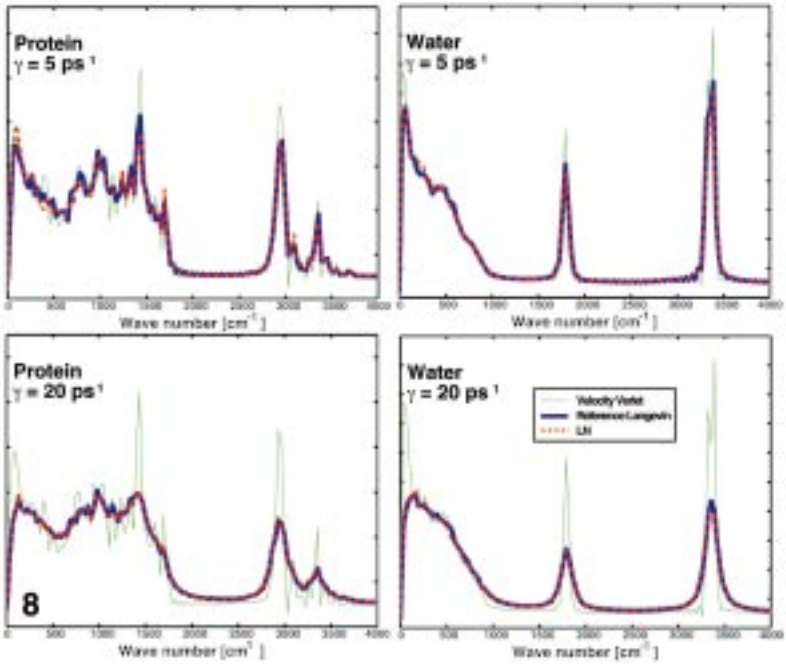

FIG. 8. BPTI spectra calculated over 5 ps runs for the protein (left) and water (right) atoms. The LN spectra ($\Delta t = 192$ fs) obtained for two γ values are compared to respective Langevin spectra (computed from reference, small-timestep Langevin trajectories) as well as to those obtained from Newtonian dynamics (integrated by Velocity Verlet).

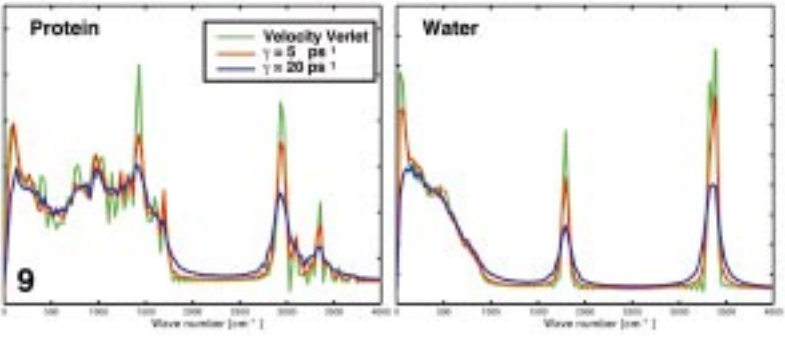

FIG. 9. BPTI spectra calculated over 5-ps runs for the protein (left) and water (right) atoms at three γ values: 0 (by Velocity Verlet) and 5 and 20 ps^{-1} (by LN; see text).

well for outer timesteps larger than 25 fs. Our recent applications of LN to a larger solvated protein and a solvated DNA dodecamer show similar performance; speedup depends on the system size, protocol used, and on the geometry of the domain used to envelop the macromolecule in the periodic-boundary-conditions protocol.

6. CONCLUSIONS

The numerical analyses and experiments reported here support the following conclusions (see also Table II).

1. The introduction of long-range forces by impulses results in severe resonances. These resonances lead to inaccurate trajectories, limit the outer timestep in Impulse-MTS methods, and hence restrict the achievable computational gain of these variants with respect to single-timestep methods. The amplitudes and widths of these resonant spikes increase with the outer timestep. Linear analysis usefully predicts the first resonant timestep to be half the fastest period; beyond this threshold, more complicated resonance patterns can develop (as seen from the 3D case). The 1D predicted values serve as good candidates for resonant timesteps in nonlinear biomolecular systems (near multiples of half the fastest period, i.e., 5, 10, 15 fs, . . .).

2. The incorporation of long-range forces by Constant Extrapolation leads to general instabilities (energy drift in practice) and resonances at odd multiples of half the fastest period, but the amplitudes of these disturbances do not grow with the outer timestep. For the linear 3D problem, as well as for general systems, the effects of generic instability seem to be stronger than the effects of resonance.

3. Splitting variants such as Extrapolation/Correction, Extended Extrapolation/Correction Cycle, Leap Extrapolation, and Midpoint Extrapolation do not appear to have much practical utility in their own right over Impulse and Constant Extrapolation because they can produce a complex array of resonances at larger outer timesteps. However, the variants Midpoint Extrapolation and Extrapolation/Correction yield better accuracy than Constant Extrapolation on a timescale less than half the fastest period. They are thus good candidates for treatment of the medium forces in biomolecules, and this is exploited in the three-class LN scheme.

4. The results obtained for Newtonian dynamics generally extend to Langevin dynamics, but a sufficiently strong coupling to the heat bath can stabilize the numerical solution and dampen resonances. For the Impulse version, the rapidly increasing amplitude of the resonances makes it very difficult to eliminate these disturbances; Constant Extrapolation is most amenable to this masking, with generic instabilities also eliminated. On the basis of

TABLE II
Resonance Summary for Splitting Variants

Method	1D resonance	1D stability	Nonlinear behavior (Langevin)
Impulse	$mT_1/2$	Stable	Resonant
Const. Extrap.	$(2m+1)T_1/2$	Mildly unstable	Mildly unstable, nonresonant
Midpt. Extrap.	$(2m+1)T_1/2$	Increasingly unstable	Good for $\Delta t < T_1/2$
E/C	$(2m+1)T_1/2$	Increasingly unstable	Good for $\Delta t < T_1/2$
EE/CC	Irregular	Increasingly unstable	Resonant
Leap Extrap.	None	Stable	Very unstable
Leap E/C	$mT_1/4$	Stable	Good for $\Delta t < T_1/4$

Note. T_1 is the fast period, Δt is the outer timestep, and m is an integer.

linear theory, we suggest guidelines for choosing minimal coupling to the heat bath (optimal γ) for the stochastic/extrapolative combination; for nonlinear systems, empirical tests are necessary and suggest the values 5–50 ps^{-1} [15].

5. While results of the 1D linear model problem provide useful resonance predictions, multidimensional linear models provide a stricter test of method feasibility. The limitation of the 1D linear model was emphasized through the Leap Extrapolation variant considered here, for which the optimistic results for the 1D linear model were misleading.

6. The stability of the MTS method depends on the protocol used and the problem. For biomolecules, a three-class splitting works better than two classes, and systems with disparate timescales are more amenable for force-splitting integrators.

7. If long-timestep stability and computational speed are important factors, and exact Hamiltonian dynamics is not required (i.e., rather, thermodynamic and conformational sampling is the goal), an effective protocol for biomolecules is a three-class Langevin MTS scheme which uses Midpoint Extrapolation for the medium forces and Constant Extrapolation for the slow forces, like LN [15]. Results here showed the effectiveness of this approach for a solvated protein model: errors in energy components and temperature are less than 3% (with respect to single-timestep Langevin trajectories) for timesteps up to 200 fs; the speedup exceeds 10; and spectral Langevin modes approximate the Newtonian modes for the coupling parameter γ in the range of 5–20 ps^{-1}.

More work is needed to overcome resonance limitations in a Newtonian framework. An interesting avenue to examine rigorously is the use of a constrained formulation for the bond stretches in combination with the MTS protocol. Though the gap in the vibrational frequency between the heavy-atom bond stretches and the light-atom bending modes is not large [20], resonance disturbances can likely be pushed further if rigid water models are used. This strategy might also be used in the LN framework to increase the maximum feasible *medium timestep* from 2 fs; this modification should not degrade the resolution quality of the medium forces but might improve the asymptotic speedup of the resulting MTS protocol, since this value is dominated by the cost of the medium forces [15].

Given the formidable sampling problem, it appears that a pragmatic balance between accuracy and long-time stability is warranted in biomolecular simulations so as to bridge the gap between theoretical and experimental biophysics; the extrapolative stochastic approach of LN analyzed here is one such compromise. See also the Schlick *et al.* review in this volume for further perspective [31].

APPENDIX A: LINEAR RESONANCE FOR IMPULSE SPLITTING

To further analyze the resonances observed, denote $\theta = \theta(\Delta\tau, \lambda_1) = \arccos(1 - \Delta\tau^2\lambda_1/2)$ and temporarily drop the arguments of P_{IV} and G for simplicity. Then (3.1) can be successively expressed as

$$\begin{aligned} A_{IV}(\Delta\tau, \lambda_1, \lambda_2, k) &= P_{IV}(A_{VV}(\Delta\tau, \lambda_1))^k P_{IV} \\ &= P_{IV}\left(G\begin{bmatrix} \cos(\theta) & \sin(\theta) \\ -\sin(\theta) & \cos(\theta) \end{bmatrix}G^{-1}\right)^k P_{IV} \\ &= P_{IV}G\begin{bmatrix} \cos(k\theta) & \sin(k\theta) \\ -\sin(k\theta) & \cos(k\theta) \end{bmatrix}G^{-1}P_{IV}. \end{aligned}$$

After some algebraic manipulations, we obtain

$$\begin{aligned} \det(A_{IV}) &= 1, \\ \text{trace}(A_{IV}) &= 2\cos(k\theta) - \frac{k\Delta\tau\lambda_2}{\sqrt{\lambda_1(1-\Delta\tau^2\lambda_1/4)}}\sin(k\theta). \end{aligned} \tag{A.1}$$

At a resonant timestep, a pair of complex conjugate eigenvalues (lying on the unit circle) becomes a real pair; hence, the condition for resonance (the same as the condition for instability) is

$$|\text{trace}(A_{IV})| > 2.$$

There are two cases in which this occurs. For analysis, let $\alpha = (\Delta\tau\lambda_2)/(2\sqrt{\lambda_1(1-\Delta\tau^2\lambda_1/4)})$ (a quantity independent of k).

Case 1. trace $(A_{IV}) < -2$. This is equivalent to

$$1 + \cos(k\theta) - k\alpha\sin(k\theta) = 2\cos^2\left(\frac{k\theta}{2}\right) - 2k\alpha\sin\left(\frac{k\theta}{2}\right)\cos\left(\frac{k\theta}{2}\right) < 0$$

or

$$\tan\left(\frac{k\theta}{2}\right) > \frac{1}{k\alpha}. \tag{A.2}$$

In particular, $\tan(k\theta/2) \to +\infty$ when

$$\frac{k\theta}{2} \approx (2m+1-\beta)\frac{\pi}{2}, \qquad m = 0, 1, 2, \ldots$$

(with β denoting a positive, small number). Since $\theta = \omega^{\text{eff}}\Delta\tau$, from (2.10) we can rewrite the above as

$$k\Delta\tau \approx \frac{2m+1-\beta}{2}\left(\frac{2\pi}{\omega_1^{\text{eff}}}\right) = (2m+1-\beta)\frac{T_1^{\text{eff}}}{2}.$$

Thus instabilities appear for outer timesteps near odd multiples of the fast (effective) half period; since $\beta > 0$ the peaks will be centered to the left of the effective half periods; as k increases, the right hand side of (A.2) decreases, so instabilities will appear for larger β's; hence the widths of the "resonant spikes" increase with k for Impulse Verlet.

To approximate the amplitude of the spikes in Case 1, note that at a resonant timestep

$$k\theta \approx (2m+1-\beta)\pi \Rightarrow \cos(m\theta) \approx -1, \qquad \sin(m\theta) \approx \beta\pi,$$

which implies

$$\text{trace}(A_{IV}) = 2\cos(k\theta) - k\alpha\sin(k\theta) \approx -2 - k\alpha\beta\pi.$$

The maximal eigenvalue is

$$r = \frac{\text{trace}(A_{IV}) - \sqrt{\text{trace}(A_{IV})^2 - 4}}{2} \approx -1 - k\frac{\alpha\beta}{2} - \sqrt{k\alpha\beta + k^2\frac{\alpha^2\beta^2}{4}} \approx -1 - k\alpha\beta,$$

where the last approximation is valid for large k. Since the nonresonant value of r is 1, the amplitudes of the resonant spikes behave like

$$|r| - 1 \approx k\alpha\beta\pi.$$

Since α is independent of k and β increases only slightly with increasing k, the spike amplitudes increase almost linearly with k.

Case 2. $\mathrm{trace}(A_{IV}) > 2$. After some algebraic manipulations, this condition is equivalent to

$$0 > \tan\left(\frac{k\theta}{2}\right) > -k\alpha, \tag{A.3}$$

implying that

$$\frac{k\theta}{2} \approx (m - \beta)\pi, \qquad 0 < \beta < \frac{1}{2},$$

or equivalently

$$k\Delta\tau \approx (m - \beta)T_1^{\mathrm{eff}}.$$

For small k, (A.3) is satisfied only by small values of β, while for large k the right hand side of (A.3) decreases and β can take larger values. This too implies that the widths of resonant spikes increase with k. This instability appears for outer timesteps near integer multiples of the effective fast period (but slightly less than mT_1^{eff}).

To approximate the spike amplitudes for Case 2, note that near a resonance we have

$$k\theta \approx (2m - \beta)\pi \Rightarrow \cos(k\theta) \approx 1, \qquad \sin(k\theta) \approx -\beta\pi.$$

An argument similar to that used above provides a linear estimate for the increasing spike height with k for large k,

$$|r| - 1 \approx k\alpha\beta\pi.$$

APPENDIX B: LINEAR RESONANCE FOR CONSTANT EXTRAPOLATION

Linear instability, or resonance, appears also with Constant Extrapolation. Since for most values of the outer timestep the spectrum of A_{CE} consists of a pair of complex conjugate eigenvalues (in general not on the unit circle [15, 11]). When the outer timestep is close to odd multiples of the fast half period the eigenvalues approach the real axis and eventually become a real pair.

To illustrate, we first bring (3.6) to a simpler form by using $\theta = \theta(\Delta\tau, \lambda_1) = \arccos(1 - \Delta\tau^2\lambda_1/2)$ and performing a change of basis. For simplicity, we temporarily omit the

arguments of the matrices G and E.

$$
\begin{aligned}
&G(\Delta\tau,\lambda_1)^{-1} \quad A_{CE}(\Delta\tau,\lambda_1,\lambda_2,k) \quad G(\Delta\tau,\lambda_1) \\
&= \begin{bmatrix} \cos(k\theta) & \sin(k\theta) \\ -\sin(k\theta) & \cos(k\theta) \end{bmatrix} + \sum_{j=0}^{k-1} \begin{bmatrix} \cos(j\theta) & \sin(j\theta) \\ -\sin(j\theta) & \cos(j\theta) \end{bmatrix} G^{-1}EG \\
&= \begin{bmatrix} \cos(k\theta) & \sin(k\theta) \\ -\sin(k\theta) & \cos(k\theta) \end{bmatrix} + \frac{\sin(k\theta/2)}{\sin(\theta/2)} \begin{bmatrix} \cos\left(\frac{k-1}{2}\theta\right) & \sin\left(\frac{k-1}{2}\theta\right) \\ -\sin\left(\frac{k-1}{2}\theta\right) & \cos\left(\frac{k-1}{2}\theta\right) \end{bmatrix} G^{-1}EG.
\end{aligned}
$$

We now introduce the quantities

$$
\begin{aligned}
a &= -\frac{\Delta\tau^2\lambda_1}{2}, \qquad b = -\frac{(1-\Delta\tau^2\lambda_1)(\Delta\tau\lambda_2)}{\sqrt{\lambda_1\left(1-\Delta\tau^2\lambda_1/4\right)}}, \\
\xi &= \operatorname{cotan}\left(\frac{\theta}{2}\right), \qquad \psi = \tan\left(\frac{k\theta}{2}\right).
\end{aligned}
$$

The trace and the determinant of the propagator A_{CE} can then be written as

$$
\operatorname{trace}(A_{CE}) = \frac{(a+b\xi-2)\psi^2 + (a\xi-b)\psi + 2}{1+\psi^2}, \tag{B.1}
$$

$$
\det(A_{CE}) = \frac{(1-a-b\xi)\psi^2 + (a\xi-b)\psi + 1}{1+\psi^2}. \tag{B.2}
$$

The discriminant of the characteristic equation for A_{CE} is then

$$
\operatorname{trace}(A_{CE})^2 - 4\cdot\det(A_{CE}) = \frac{\psi^2}{(1+\psi^2)^2}\left(\alpha_1\psi^2 + \alpha_2\psi + \alpha_3\right), \tag{B.3}
$$

where

$$
\begin{aligned}
\alpha_1 &= (a+b\xi)^2 \geq 0, \\
\alpha_2 &= 2a\xi(a+b) - 8(a\xi+b) - 2b(a+b\xi), \\
\alpha_3 &= (a\xi+b)^2 + 8(a+b\xi) - 16.
\end{aligned}
$$

Resonance occurs for values of ψ for which the quadratic function in (B.3) is positive; since the dominant coefficient is positive, the function is positive when $\psi \to -\infty$ or $\psi \to +\infty$, or when

$$
\frac{k\theta}{2} \approx (2m+1)\frac{\pi}{2}.
$$

This is equivalent to

$$
k\Delta\tau \approx (2m+1)\frac{T_1^{\text{eff}}}{2}.
$$

Note that, since both plus and minus infinity give resonance, the spikes will be centered around odd multiples of the effective half period.

For $k\Delta\tau \approx mT^{\text{eff}}$ we have $\psi \approx 0$ and resonance appears if and only if $\alpha_3 > 0$. But for $\Delta\tau \ll T_1^{\text{eff}}$ one has $(a\xi + b)^2 = \mathcal{O}(\Delta\tau^2)$, $a = \mathcal{O}(\Delta\tau^2)$, $b\xi = -\lambda_2/\lambda_1 + \mathcal{O}(\Delta\tau)$, and $\alpha_3 < 0$ follows.

To analyze the amplitudes of the resonant spikes for Constant Extrapolation, we define

$$r_{1,2} = \frac{\text{trace}(A_{CE}) \pm \sqrt{\text{trace}(A_{CE})^2 - 4\det(A_{CE})}}{2}.$$

Near resonances, $\psi \to \pm\infty$, implying

$$r_1 \to -1, \qquad r_2 \to -1 + a + b\xi,$$

with both limits independent of k. *This explains the remarkable fact that the spike amplitudes are independent of k for extrapolation methods*. The smallest (in absolute value) eigenvalue has a "peak" at -1, which is in excellent agreement with the numerical results of Barth and Schlick [15, 11]. The largest (in absolute value) eigenvalue has peaks at

$$|r_2| = 1 + \frac{\Delta\tau^2\lambda_1}{2} + \Delta\tau\lambda_2 \frac{1 - \Delta\tau\lambda_1}{\sqrt{\lambda_1\left(1 - \Delta\tau^2\lambda_1/4\right)}} \operatorname{cotan}\left(\frac{\theta}{2}\right).$$

For the limit case $\Delta\tau \to 0$ we have

$$\Delta\tau \cdot \operatorname{cotan}\left(\frac{\theta}{2}\right) = \Delta\tau \cdot \operatorname{cotan}\left(\frac{\omega_1^{\text{eff}}\Delta\tau}{2}\right) \approx \frac{2}{\omega_1^{\text{eff}}} \approx \frac{2}{\sqrt{\lambda_1}},$$

and hence

$$|r_2| \approx 1 + 2\frac{\lambda_2}{\lambda_1}.$$

The (nonresonant) peak value of the spectral radius of A_{CE} can be estimated roughly as

$$\rho(A_{CE}) \approx \frac{|r_1| + |r_2|}{2} \approx 1 + \frac{\lambda_2}{\lambda_1}.$$

This confirms the empirical relations of Barth and Schlick [15, 11] for the magnitude of the instability.

The nonresonance value for $k\Delta\tau = mT_1^{\text{eff}}$ can be readily obtained by noticing that $\psi = 0$ in this case. Hence $\det(A_{CE}) = 1$, $\text{trace}(A_{CE}) = 2$, and $r_1 = r_2 = 1$. This result is also confirmed by numerical experiments.

As for the asymptotic interpretation, for small inner timesteps $\Delta\tau \to 0$, any discretization using Constant Extrapolation approximately solves the system

$$\begin{bmatrix} \dot{X} \\ \dot{V} \end{bmatrix} = \begin{bmatrix} V \\ -\lambda_1 X - \lambda_2 X^0 \end{bmatrix}$$

for $0 \le t \le k\Delta\tau$ with $X(0) = X^0$, $V(0) = V^0$. This system has the analytic solution

$$\begin{bmatrix} X(k\Delta\tau) \\ V(k\Delta\tau) \end{bmatrix} = A_{CE}^{\text{a}}(k\Delta\tau, \lambda_1, \lambda_2) \begin{bmatrix} X^0 \\ V^0 \end{bmatrix}$$

with

$$A^{\mathrm{a}}_{CE}(k\Delta\tau,\lambda_1,\lambda_2)=\begin{bmatrix}\left(1+\frac{\lambda_2}{\lambda_1}\right)C-\frac{\lambda_2}{\lambda_1} & \frac{1}{\sqrt{\lambda_1}}S\\ -\sqrt{\lambda_1}\left(1+\frac{\lambda_2}{\lambda_1}\right)S & C\end{bmatrix},$$

where

$$S=\sin(\sqrt{\lambda_1}k\Delta\tau),\qquad C=\cos(\sqrt{\lambda_1}k\Delta\tau). \tag{B.4}$$

For determining the eigenvalues, we calculate

$$\begin{aligned}\operatorname{trace}\left(A^{\mathrm{a}}_{CE}\right)&=\left(2+\frac{\lambda_2}{\lambda_1}\right)C-\frac{\lambda_2}{\lambda_1},\\ \det\left(A^{\mathrm{a}}_{CE}\right)&=1+\frac{\lambda_2}{\lambda_1}(1-C),\\ \operatorname{trace}\left(A^{\mathrm{a}}_{CE}\right)^2-4\det\left(A^{\mathrm{a}}_{CE}\right)&=4\sin^4\left(\frac{\sqrt{\lambda_1}k\Delta\tau}{2}\right)\left\{\frac{\lambda_2^2}{\lambda_1^2}-4\left(1+\frac{\lambda_2}{\lambda_1}\right)\operatorname{cotan}^2\left(\frac{\sqrt{\lambda_1}k\Delta\tau}{2}\right)\right\}.\end{aligned}$$

From here we see that the spectrum is real (which implies resonance) for

$$\operatorname{cotan}\left(\frac{\sqrt{\lambda_1}k\Delta\tau}{2}\right)\approx 0,$$

i.e., for outer timesteps approximately equal to odd multiples of the fast half period,

$$k\Delta\tau\approx(2m+1)\frac{\pi}{\sqrt{\lambda_1}}=(2m+1)\frac{T_1}{2}.$$

For these values of the outer timestep, A^{a}_{CE} has two real eigenvalues, namely -1 and $-1-2\lambda_2/\lambda_1$. These eigenvalues do not depend on $k\Delta\tau$, as noticed previously.

APPENDIX C: LINEAR RESONANCE FOR MIDPOINT EXTRAPOLATION

A derivation similar to the Constant Extrapolation case is possible; here we only present the asymptotic approximation. For small inner timesteps $\Delta\tau\to 0$, one Midpoint Extrapolation step approximates the solution of the system

$$\begin{bmatrix}\dot{X}\\ \dot{V}\end{bmatrix}=\begin{bmatrix}V\\ -\lambda_1 X-\lambda_2 X^E\end{bmatrix}$$

for $0\le t\le k\Delta\tau$ with $X(0)=X^0$, $V(0)=V^0$, $X^E=X^0+(k\Delta\tau/2)V^0$. This system has the analytic solution

$$\begin{bmatrix}X(k\Delta\tau)\\ V(k\Delta\tau)\end{bmatrix}=A^{\mathrm{a}}_{ME}(k\Delta\tau,\lambda_1,\lambda_2)\begin{bmatrix}X^0\\ V^0\end{bmatrix}$$

with

$$A^{\mathrm{a}}_{ME}(k\Delta\tau,\lambda_1,\lambda_2)=\begin{bmatrix}\left(1+\frac{\lambda_2}{\lambda_1}\right)C-\frac{\lambda_2}{\lambda_1} & \frac{1}{\sqrt{\lambda_1}}S-\frac{k\Delta\tau}{2}\frac{\lambda_2}{\lambda_1}(1-C)\\ -\sqrt{\lambda_1}\left(1+\frac{\lambda_2}{\lambda_1}\right)S & C-\frac{k\Delta\tau}{2}\frac{\lambda_2}{\sqrt{\lambda_1}}S\end{bmatrix},$$

where we used S and C as defined in (B.4). For determining the eigenvalues, we calculate

$$\begin{aligned}\operatorname{trace}\left(A^{\mathrm{a}}_{ME}\right)&=\left(2+\frac{\lambda_2}{\lambda_1}\right)C-\frac{\lambda_2}{\lambda_1}-\frac{k\Delta\tau}{2}\frac{\lambda_2}{\sqrt{\lambda_1}}S,\\ \det\left(A^{\mathrm{a}}_{ME}\right)&=1+\frac{\lambda_2}{\lambda_1}(1-C)-\frac{k\Delta\tau}{2}\frac{\lambda_2}{\sqrt{\lambda_1}}S,\end{aligned}$$

$$\begin{aligned}&\operatorname{trace}\left(A^{\mathrm{a}}_{ME}\right)^2-4\det\left(A^{\mathrm{a}}_{ME}\right)\\ &=4\sin^4\left(\frac{\sqrt{\lambda_1}k\Delta\tau}{2}\right)\left\{\frac{\lambda_2^2}{\lambda_1^2}-4\left(1+\frac{\lambda_2}{\lambda_1}-\frac{k^2\Delta\tau^2\lambda_2^2}{16\lambda_1}\right)\operatorname{cotan}^2\left(\frac{\sqrt{\lambda_1}k\Delta\tau}{2}\right)\right.\\ &\quad\left.+k\Delta\tau\frac{\lambda_2}{\sqrt{\lambda_1}}\left(2+\frac{\lambda_1}{\lambda_2}\right)\operatorname{cotan}\left(\frac{\sqrt{\lambda_1}k\Delta\tau}{2}\right)\right\}.\end{aligned}$$

For outer timesteps near odd multiples of the fast half period

$$k\Delta\tau\approx(2m+1-\beta)\frac{\pi}{\sqrt{\lambda_1}}=(2m+1-\beta)\frac{T_1}{2},$$

where β is a small nonnegative number, it holds that

$$\operatorname{cotan}\left(\frac{\sqrt{\lambda_1}k\Delta\tau}{2}\right)\approx\frac{\beta\pi}{2},$$

and the spectrum is real. The two eigenvalues are (to first order in β) $-1+k\Delta\tau\sqrt{\lambda_1}\beta\pi/2$ and $-1-2\lambda_2/\lambda_1-k\Delta\tau(1-\lambda_2/\lambda_1)\sqrt{\lambda_1}\beta\pi/2$; this implies that the instability grows linearly with increasing outer timestep.

APPENDIX D: SYMPLECTIC HYBRID IMPULSE/EXTRAPOLATION METHODS

Consider the system

$$\begin{bmatrix}\dot X\\ \dot V\end{bmatrix}=\begin{bmatrix}V\\ -M^{-1}\nabla E_S(X)-M^{-1}\nabla E_F(X)\end{bmatrix},$$

where $E_S(X)$, $E_F(X)$ denote the potential energies associated with the slow and the fast forces, respectively.

Split the system into its slow and fast components

$$\begin{bmatrix}\dot X\\ \dot V\end{bmatrix}=\begin{bmatrix}0\\ -M^{-1}\nabla E_S(X)\end{bmatrix}+\begin{bmatrix}V\\ -M^{-1}\nabla E_F(X)\end{bmatrix}$$

and apply Velocity Verlet to each of the above subsystems, in Strang order with steps $k\Delta\tau$ and τ, respectively. This means that one takes a $k\Delta\tau/2$ step for the slow subsystem, k steps

with the stepsize $\Delta\tau$ for the fast subsystem, and finally another $k\Delta\tau/2$ step for the slow subsystem. The resulting method is Impulse Verlet.

We now add and subtract an "extrapolation potential" $A(X)$, which can be thought of as a computationally cheap approximation to $E_S(X)$ [13]. This gives the splitting

$$\begin{bmatrix} \dot{X} \\ \dot{V} \end{bmatrix} = \begin{bmatrix} 0 \\ -M^{-1}\nabla E_S(X) + M^{-1}\nabla A(X) \end{bmatrix} + \begin{bmatrix} V \\ -M^{-1}\nabla E_F(X) - M^{-1}\nabla A(X) \end{bmatrix}.$$

Both the slow and the fast subsystems are Hamiltonian, with their respective Hamiltonian functions

$$H_S = E_S(X) - A(X), \qquad H_F = \tfrac{1}{2}V^T MV + E_F(X) + A(X).$$

Approximating the original system by a half-step integration of the slow part, followed by a full step integration of the fast part, and again a half-step integration of the slow part is a composition of symplectic flows; hence it is symplectic. Moreover, this approximates the original flow to second order because of the symmetry of the composition.

The simplest choice is a linear extrapolation potential, which gives rise to a constant extrapolation force, where $A(X) = \mathcal{E}^T X$, $\nabla A(X) = \mathcal{E}$.

APPENDIX E: LINEAR RESONANCE FOR EXTRAPOLATION/CORRECTION

Let

$$\theta = \arccos\left(1 - \frac{\Delta\tau^2\lambda_1}{2}\right), \qquad \zeta = -\frac{k\Delta\tau}{2}\lambda_2 \frac{\sin(k\theta)}{\sqrt{\lambda_1\left(1 - \Delta\tau^2\lambda_1/4\right)}}.$$

Using the notation introduced above and defining p implicitly,

$$\zeta = -\frac{k\Delta\tau\lambda_2}{\sqrt{\lambda_1\left(1 - \Delta\tau^2\lambda_1/4\right)}} \frac{\psi}{1+\psi^2} = \frac{kp\psi}{1+\psi^2},$$

we have

$$\mathrm{trace}(A_{E/CV}) = \mathrm{trace}(A_{CE}) + \zeta = \frac{(a + b\xi - 2)\psi^2 + (a\xi - b + kp)\psi + 2}{1+\psi^2},$$

$$\det(A_{E/CV}) = \det(A_{CE}) + \zeta = \frac{(1 - a - b\xi)\psi^2 + (a\xi - b + kp)\psi + 1}{1+\psi^2}.$$

The discriminant of the characteristic equation for $A_{E/CV}$ is then

$$\mathrm{trace}(A_{CE})^2 - 4 \cdot \det(A_{CE}) = \frac{\psi^2}{(1+\psi^2)^2}(\hat{\alpha}_1\psi^2 + \hat{\alpha}_2\psi + \hat{\alpha}_3), \tag{E.1}$$

$$\begin{aligned} \hat{\alpha}_1 &= (a + b\xi)^2 \geq 0 \\ \hat{\alpha}_2 &= 2a\xi(a+b) - 8(a\xi + b) - 2b(a + b\xi) + 2kp(a + b\xi - 2) \\ \hat{\alpha}_3 &= (a\xi + b)^2 + 8(a + b\xi) - 16 + k^2p^2 + 2kp(a\xi - b). \end{aligned}$$

An argument similar to that used for Constant Extrapolation produces the resonance condition

$$k\Delta\tau \approx (2m+1)\frac{T_1^{\text{eff}}}{2}.$$

Again the spikes are centered around odd multiples of the effective half period.

For $k\Delta\tau \approx mT^{\text{eff}}$ we have $\psi \approx 0$ and resonance appears if and only if $\hat{\alpha}_3 > 0$. Unlike Constant Extrapolation, this situation is possible for large values of k. The resonance at $k\Delta\tau \approx mT^{\text{eff}}$ is then part of either the $(m-1/2)T^{\text{eff}}$ resonant spike or the $(m+1/2)T^{\text{eff}}$ one.

To estimate the amplitude of the resonant Extrapolation/Correction spikes, we remark that the analysis is complicated by the k-dependency of the coefficients of the quadratic function in (E.1), unlike in Constant Extrapolation. A rough estimate can be obtained as follows. Let $k_1, k_2, \ldots$ be an increasing sequence of k's for which the corresponding ψ's are uniformly bounded: $|\psi| < M$, where M is large but finite. It can be shown that the peaks of the resonant spike for a large k_j are approximately $k_j p/M$ in height; in other words, we expect an almost linear increase in the amplitude of the spikes. This is similar to Impulse Verlet and in sharp contrast to Constant Extrapolation (where the spike heights are constant).

Consider now k values satisfying

$$\frac{k\theta}{2} \approx m\pi + \frac{\pi}{4} \quad \Leftrightarrow \quad \psi = 1.$$

It can be easily shown that for these outer steps $A_{E/CV}$ has a pair of complex conjugate (non-resonant) eigenvalues, of modulus increasing like $kp/4$; this result is confirmed by the numerical tests. For the asymptotic interpretation, let $C = \cos(\sqrt{\lambda_1}k\Delta\tau)$, $S = \sin(\sqrt{\lambda_1}k\Delta\tau)$. In analogy to the asymptotic behavior of Constant Extrapolation, we obtain

$$\begin{aligned} A^{\text{a}}_{E/CV}(k\Delta\tau,\lambda_1,\lambda_2) &= (I + E_{E/CV}(\Delta\tau,\lambda_2,k))A^{\text{a}}_{CE}(k\Delta\tau,\lambda_1,\lambda_2) - E_{E/CV}(\Delta\tau,\lambda_2,k) \\ &= \begin{bmatrix} \left(1+\frac{\lambda_2}{\lambda_1}\right)C - \frac{\lambda_2}{\lambda_1} & \frac{1}{\sqrt{\lambda_1}}S \\ \frac{k\Delta\tau\lambda_2}{2} - \frac{k\Delta\tau\lambda_2^2}{2\lambda_1}C - \left(\sqrt{\lambda_1} + \frac{\lambda_2}{\sqrt{\lambda_1}}\right)S & C - \frac{k\Delta\tau\lambda_2}{2\sqrt{\lambda_1}}S \end{bmatrix}. \end{aligned}$$

ACKNOWLEDGMENT

We thank Daniel Strahs for setting the solvated BPTI model in CHARMM and for related valuable discussions. We are grateful to Wei Xu for technical assistance with the manuscript and figure preparation.

REFERENCES

1. Y. Duan and P. A. Kollman, Pathways to a protein folding intermediate observed in a 1-microsecond simulation in aqueous solution, *Science* **282**, 740 (1998).
2. L. Verlet, Computer experiments on classical fluids. I. Thermodynamical properties of Lennard-Jones molecules, *Phys. Rev.* **159**, 98 (1967).
3. J. M. Sanz-Serna and M. P. Calvo, *Numerical Hamiltonian Problems* (Chapman & Hall, London, 1994).
4. W. B. Street, D. J. Tildesley, and G. Saville, Multiple time step methods in molecular dynamics, *Mol. Phys.* **35**, 639 (1978).

5. R. D. Swindoll and J. M. Haile, A multiple time step method for molecular dynamics simulations of fluids of chain molecules, *J. Chem. Phys.* **53**, 289 (1984).
6. M. Tuckerman, B. J. Berne, and G. J. Martyna, Reversible multiple time scale molecular dynamics, *J. Chem. Phys.* **97**, 1990 (1992).
7. H. Grubmuller, H. Heller, A. Windemuth, and K. Schulten, Generalized Verlet algorithm for efficient molecular dynamics simulations with long-range interactions, *Mol. Sim.* **6**, 121 (1991).
8. R. Zhou and B. J. Berne, A new molecular dynamics method combining the reference system propagator algorithm with a fast multipole method for simulating proteins and other complex systems, *J. Chem. Phys.* **103**, 9444 (1995).
9. M. Watanabe and M. Karplus, Simulations of macromolecules by multiple time-step methods, *J. Chem. Phys.* **99**, 5680 (1995).
10. J. J. Biesiadecki and R. D. Skeel, Dangers of multiple time step methods, *J. Comput. Phys.* **109**, 318 (1993).
11. E. Barth and T. Schlick, Extrapolation versus impulse in multiple-timestepping schemes. II. linear analysis and applications to Newtonian and Langevin dynamics, *J. Chem. Phys.* **109**, 1632 (1998).
12. M. Mandziuk and T. Schlick, Resonance in the dynamics of chemical systems simulated by the implicit-midpoint scheme, *Chem. Phys. Lett.* **237**, 525 (1995).
13. R. D. Skeel, G. Zhang, and T. Schlick, A family of symplectic integrators: Stability, accuracy, and molecular dynamics applications, *SIAM J. Sci. Comput.* **18**, 202 (January 1997).
14. T. Schlick, M. Mandziuk, R. D. Skeel, and K. Srinivas, Nonlinear resonance artifacts in molecular dynamics simulations, *J. Comput. Phys.* **139**, 1 (1998).
15. E. Barth and T. Schlick, Overcoming stability limitations in biomolecular dynamics. I. Combining force splitting via extrapolation with Langevin dynamics in LN, *J. Chem. Phys.* **109**, 1617 (1998).
16. S. Broyde and B. E. Hingerty, Effective computational strategies for determining structures of carcinogen damaged DNA, *J. Comput. Phys.* **151**, 313 (1999).
17. L. S. D. Caves, J. D. Evanseck, and M. Karplus, Locally accessible conformations of proteins: Multiple molecular dynamics simulations of crambin, *Protein Sci.* **7**, 649 (1998).
18. G. Zhang and T. Schlick, LIN: A new algorithm combining implicit integration and normal mode techniques for molecular dynamics, *J. Comput. Chem.* **14**, 1212 (1993).
19. G. Zhang and T. Schlick, The Langevin/Implicit-Euler/Normal-Mode scheme (LIN) for molecular dynamics at large time steps, *J. Chem. Phys.* **101**, 4995 (1994).
20. T. Schlick, E. Barth, and M. Mandziuk, Biomolecular dynamics at long timesteps: Bridging the timescale gap between simulation and experimentation, *Annu. Rev. Biophys. Biomol. Struc.* **26**, 179 (1997).
21. B. Garcia-Archilla, J. M. Sanz-Serna, and R. D. Skeel, Long-time-step methods for oscillatory differential equations, Technical Report 7, Dept. Math. Applic. Comp., University of Valladolid (1996).
22. M. E. Tuckerman, B. J. Berne, and G. J. Martyna, Molecular dynamics algorithm for multiple time scales: Systems with long range forces, *J. Chem. Phys.* **94**, 6811 (1991).
23. J. L. Scully and J. Hermans, Multiple time steps: Limits on the speed-up of molecular dynamics simulations of aqueous systems, *Mol. Sim.* **11**, 67 (1993).
24. G. D. Quinlan and S. Tremaine, Symmetric multistep methods for the numerical integration of planetary orbits, *Astrophys. J.* **100**, 1692 (1990).
25. T. Schlick, S. Figueroa, and M. Mezei, A molecular dynamics simulation of a water droplet by the implicit Euler/Langevin scheme, *J. Chem. Phys.* **94**, 2118 (1991).
26. T. Schlick and A. Fogelson A truncated Newton minimization package for large-scale problems. I. Algorithm and usage, *ACM Trans. Math. Software* **14**, 46 (1992).
27. T. Schlick and A. Fogelson, A truncated Newton minimization package for large-scale problems. II. Implementation examples, *ACM Trans. Math. Software* **14**, 71 (1992).
28. D. Xie and T. Schlick, Efficient implementation of the truncated Newton algorithm for large-scale chemistry applications, *SIAM J. Optim.* **9** (1999); see also Xie and Schlick in *ACM Trans. Math. Software* **25** (1999).
29. B. R. Brooks, R. E. Bruccoleri, B. D. Olafson, D. J. States, S. Swaminathan, and M. Karplus, CHARMM: A program for macromolecular energy, minimization, and dynamics calculations, *J. Comput. Chem.* **4**, 187 (1983).

30. A. D. MacKerell, Jr., D. Bashford, M. Bellott, R. L. Dunbrack, Jr., J. D. Evanseck, M. J. Field, S. Fischer, J. Gao, H. Guo, S. Ha, D. Joseph-McCarthy, L. Kuchnir, K. Kuczera, F. T. K. Lau, C. Mattos, S. Michnick, T. Ngo, D. T. Nguyen, B. Prodhom, W. E. Reiher III, B. Roux, M. Schlenkrich, J. C. Smith, R. Stote, J. Straub, M. Watanabe, J. Wiorkiewicz-Kuczera, D. Yin, and M. Karplus, All-atom empirical potential for molecular modeling and dynamics studies of proteins, *J. Phys. Chem.* **102**, 3586 (1998).

31. T. Schlick, R. D. Skeel, A. T. Brünger, L. V. Kalé, J. A. Board, Jr., J. Hermans, and K. Schulten, Algorithmic challenges in computational molecular biophysics, *J. Comput. Phys.* **151**, 9 (1999).